
Learning under Distributional Drift: Prequential Reproducibility as an Intrinsic Statistical Resource

Sofiya Zaichyk¹

¹Innovative Defense Technologies (IDT)

Abstract

Statistical learning under distributional drift remains poorly characterized, especially in closed-loop settings where learning alters the data-generating law. We introduce an intrinsic drift budget C_T that quantifies the cumulative *information-geometric* motion of the data distribution along the realized learner–environment trajectory, measured in Fisher–Rao distance (the Riemannian metric induced by Fisher information on a statistical manifold of data-generating laws). The budget decomposes this motion into exogenous change (environmental drift that would occur without intervention) and policy-sensitive feedback contributions (drift induced by the learner’s actions through the closed loop). This yields a rate-based characterization: in prequential reproducibility bounds—where performance on the realized stream is used to predict one-step-ahead performance under the next distribution—the drift contribution enters through the *average drift rate* C_T/T , i.e., normalized cumulative Fisher–Rao motion per time step. We prove a drift–feedback bound of order $T^{-1/2} + C_T/T$ (up to a controlled second-order remainder) and establish a matching minimax lower bound on a canonical subclass, showing this dependence is tight up to constants. Consequently, when C_T/T is nonnegligible, one-step-ahead reproducibility admits an irreducible accuracy floor of the same order. Finally, the framework places exogenous drift, adaptive data analysis, and performative feedback within a common geometric account of distributional motion.

Keywords: information geometry; statistical learning theory; non-stationary learning; generalization bounds; distribution shift; closed-loop learning

1 Introduction

Modern learning systems often operate in *self-modifying environments*, where learning alters the very distribution it learns from. A recommender policy reshapes user preferences as it updates (Perdomo et al., 2020); adaptive experiments change the distribution from which subsequent data are drawn (Li et al., 2024); and reinforcement-driven agents modify the state transitions that determine future feedback (Sutton and Barto, 2018; Even-Dar and Mansour, 2003). In all such cases, the learner is not a passive observer of a stationary process but an active participant in an evolving distributional flow. This introduces a key problem. The feedback coupling breaks not only stationarity, but the i.i.d. sampling premise underlying classical generalization theory (Vapnik, 1998).

1.1 Motivation

Given samples $\{(x_i, y_i)\}_{i=1}^T$ drawn i.i.d. from a fixed distribution $p(x, y)$, population and empirical risks coincide asymptotically, with convergence rate $O(T^{-1/2})$ (Vapnik, 1998). Once the data-generating process itself changes, these guarantees collapse, and the population quantity being

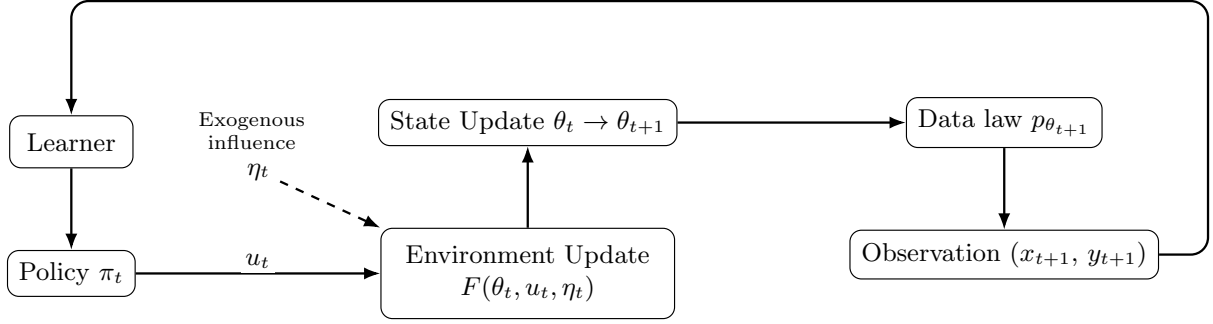


Figure 1: The learner’s policy π_t and exogenous influence η_t act on the environment, evolving θ_t to θ_{t+1} under $F(\theta_t, u_t, \eta_t)$. This new state defines the next data distribution $p_{\theta_{t+1}}$, closing the feedback loop. Exogenous factors η_t perturb θ_t externally, while endogenous feedback arises from the learner’s own actions.

estimated becomes path-dependent. In such settings, the limiting factor is not only sample size, but the average *one-step* change in the data-generating law.

To make this concrete, consider an adaptive recommender with policy π_t that selects content while updating its model from observed responses. Each recommendation depends on past data yet also shapes future data, since user preferences evolve with exposure. Let the environment be parameterized by θ_t , governing $p_{\theta_t}(x, y)$, and evolve in closed loop according to $\theta_{t+1} = F(\theta_t, u_t, \eta_t)$, where u_t is some action chosen from a learned policy and η_t denotes exogenous influences. Even when F is smooth and deterministic conditional on (u_t, η_t) , its dependence on u_t couples learning to the data-generating law. The induced distributions $p_{\theta_1}, p_{\theta_2}, \dots$ trace a distributional trajectory. To reason about how rapidly this trajectory changes, we need a notion of *local* statistical displacement between nearby p_θ ’s. The family $\{p_\theta\}$ forms a statistical manifold whose intrinsic Riemannian metric—the Fisher information—measures how sensitively the distribution changes under infinitesimal perturbations of θ . Thus the learner–environment interaction induces geometric motion in Fisher–Rao distance, and the realized sequence $\{(x_t, y_t)\}$ need not be stepwise self-consistent. Even when the learner’s update rule is fixed, the coupled dynamics can move the underlying law p_{θ_t} enough that performance measured at time t is not predictive of performance under $p_{\theta_{t+1}}$. When Fisher–Rao motion accumulates rapidly, successive distributions become poorly aligned, degrading prequential (one-step-ahead) evaluation.

The same feedback-driven coupling arises in adaptive testing, model-in-the-loop simulation, and autonomous control. This raises a basic question: how rapidly can the learner–environment system move before classical guarantees break? To answer this, we develop a geometric framework for quantifying distributional motion during learning. We then relate this motion to nonasymptotic generalization and prequential reproducibility under drift.

1.2 Conceptual View

We view the data-generating process as a trajectory $\{\theta_t\}$ on a statistical manifold (Θ, g_θ) endowed with the Fisher–Rao metric (Amari and Nagaoka, 2000). Any smooth divergence admits a second-order expansion whose Hessian defines a local Riemannian metric (Amari, 2016). For the broad class of f -divergences, including KL, χ^2 , Hellinger, and α -divergences, this induced metric coincides with the Fisher–Rao geometry. Fisher–Rao is therefore the natural information-geometric metric

on a statistical model family (Čencov, 1982; Amari and Nagaoka, 2000), capturing displacement intrinsic to the family rather than to a particular coordinate system. In particular, Fisher–Rao is the unique Riemannian metric on parametric families that is invariant under smooth reparameterizations (Čencov, 1982). Because drift unfolds along a realized trajectory, we need a cumulative measure of motion that composes across time. Once a local geometry g_θ is fixed, the natural choice is arc length, $\int \|\dot{\theta}(t)\|_{g_{\theta(t)}} dt$, which is additive under concatenation of path segments. Taking g_θ to be Fisher–Rao thus yields an intrinsic scale for describing how small distributional perturbations alter the statistical environment of a learner.

In discrete time, the intrinsic Fisher–Rao path length of the realized trajectory is

$$\mathcal{A}_T := \sum_{t=1}^T d_F(\theta_{t+1}, \theta_t), \quad (1)$$

where d_F is the Fisher–Rao geodesic distance. This is conceptually distinct from aggregating pairwise TV, Wasserstein, or KL discrepancies. Those are pairwise divergences not an intrinsic line element whose path integral yields a coordinate-free notion of cumulative motion. What \mathcal{A}_T measures is not merely “how far the distribution moved” in a chosen divergence, but the total intrinsic statistical displacement expended along the trajectory in the unique local geometry that governs estimation.

Cumulative vs. per-step motion. The path length \mathcal{A}_T is cumulative and may grow even when the trajectory stays in a bounded region. Prequential reproducibility is assessed step-to-step, so the operative control in our bounds is the *average* motion rate \mathcal{A}_T/T (and its proxy C_T/T), which captures how rapidly adjacent laws change.

Definition 1 (Prequential reproducibility and intrinsic drift budget). *Prequential reproducibility is an evaluation property of learning under an evolving data-generating law: the extent to which performance measured on the realized data stream remains predictive of performance under the next data-generating distribution along the trajectory. In Section 3 we formalize this as a gap between empirical evaluation and a one-step-ahead (prequential) population target.*

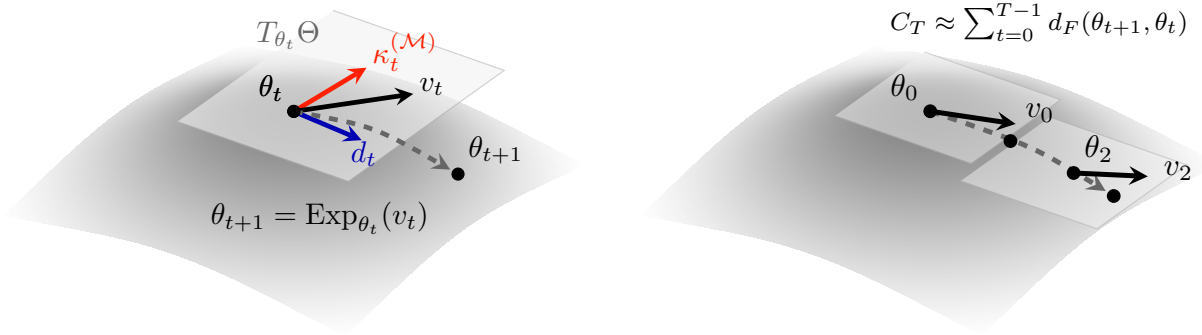
We summarize cumulative distributional motion by a tractable intrinsic drift budget

$$C_T := \sum_{t=1}^T (d_t + \alpha \kappa_t^{(\mathcal{M})}), \quad (2)$$

where d_t captures exogenous drift and $\kappa_t^{(\mathcal{M})}$ captures the leading-order policy-sensitive contribution in Fisher geometry. In Sections 3–4 we prove that C_T controls the intrinsic Fisher–Rao path length \mathcal{A}_T up to a controlled second-order remainder. Accordingly, our prequential reproducibility bounds depend on the budget through the average rate C_T/T .

While the intrinsic motion \mathcal{A}_T depends only on the realized trajectory, the budget C_T isolates *why* the trajectory moves. Some motion is *exogenous*, driven by external change, while the remainder is *endogenous*, reflecting how the learner’s policy alters the data-generating law. This decomposition is carried out within the same Fisher geometry and is tied to local control-to-distance comparisons along the realized trajectory. A visual illustration is provided in Figure 2.

Coupling and effective drift. Because the target is one-step-ahead, our bounds depend on motion through the average rate C_T/T . In feedback-driven settings this rate is not merely a property



(a) Local drift decomposition in a tangent space. (b) Global Fisher–Rao path length \mathcal{A}_T and proxy budget C_T .

Figure 2: Geometric intuition for learning under drift. (a) At each step the environment parameter θ_t lies on the statistical manifold (Θ, g_θ) . Local motion decomposes into an *exogenous* component (captured by d_t) and a *policy-sensitive* component (captured by $\kappa_t^{(\mathcal{M})}$), defined using local Fisher geometry around the baseline next state. (b) Iterating these local movements generates a global Fisher–Rao trajectory $\theta_1 \rightarrow \theta_2 \rightarrow \dots \rightarrow \theta_{T+1}$, whose intrinsic length $\mathcal{A}_T = \sum_{t=1}^T d_F(\theta_{t+1}, \theta_t)$ measures total statistical motion. The proxy budget $C_T = \sum_{t=1}^T (d_t + \alpha \kappa_t^{(\mathcal{M})})$ provides a tractable upper-bounding surrogate for \mathcal{A}_T up to higher-order remainder terms, and its normalization C_T/T is the operational quantity that appears in our prequential reproducibility bounds. This normalization is what shows up in the theorems.

of an exogenous drift path. Policies that stably summarize the environment can reduce the effective one-step change, whereas policies that continually chase transient fluctuations can sustain large per step motion and incur a larger penalty. The point is not that motion must be small in total. Prequential reproducibility degrades when the coupled dynamics spend budget quickly.

Our main results relate the drift-induced component of prequential behavior to the average motion rate C_T/T , and we prove a matching minimax lower bound on a canonical subclass establishing a prequential reproducibility speed limit of order $\Theta(T^{-1/2} + C/T)$.

1.3 Relation to Prior Frameworks

Several established frameworks capture pieces of the broader picture studied here. While each captures an important aspect of instability, the difficulty is that these pieces are usually treated in isolation. Our work provides a geometric viewpoint that connects them.

Stationary learning (Vapnik, 1998; Shalev-Shwartz and Ben-David, 2014) assumes fixed $p(x, y)$ and produces the familiar $O(T^{-1/2})$ convergence guarantees derived from concentration under i.i.d. sampling. *Nonstationary stochastic optimization* (Besbes et al., 2015) introduces a variation budget that measures how much the target distribution can change exogenously over time, typically through a cumulative constraint such as $\sum_{t=1}^{T-1} d(p_{\theta_{t+1}}, p_{\theta_t}) \leq V_T$ for a discrepancy d (often total variation or Wasserstein). Such budgets constrain external motion but they do not model endogenous coupling to the learner’s policy, nor do they encode how drift is distributed over time. In contrast, our bounds control prequential reproducibility through an *average drift rate* C_T/T derived from intrinsic Fisher–Rao motion along the realized trajectory, and in feedback-driven settings this rate can itself depend on the learner’s actions. Related approaches bound performance under drifting distributions using stability or Rademacher techniques (Blanchard et al., 2021; Kuznetsov and Mohri, 2016;

Mohri and Muñoz Medina, 2012) but likewise do not explicitly model feedback between learner and environment. PAC–Bayes analyses have also been developed for distributional change, notably in the domain adaptation setting of Germain et al. (2016). However, those results bound a single *source–target shift*, whereas the present work studies *path-dependent*, cumulative drift induced by sequential learner–environment coupling.

Performative prediction (Perdomo et al., 2020) explicitly introduces feedback between model and environment, focusing on equilibrium conditions where that feedback vanishes ($p_{\theta_{t+1}} \approx p_{\theta_t}$). Follow-up work has refined aspects of this coupling (Izzo et al., 2021; Jagadeesan et al., 2022), but continues to analyze convergence to fixed points rather than the explicit accumulation of temporal drift. *Adaptive data analysis* (Dwork et al., 2015; Rogers et al., 2020; Russo and Zou, 2016; Bassily et al., 2016) addresses feedback in the statistical query setting and bounds overfitting through mutual-information or stability arguments, yet does so within a static population that does not itself evolve.

These approaches define distinct ways to measure instability: sample variance, variation budgets, equilibrium deviation, and information flow. The present work connects them by treating drift as motion on a statistical manifold. The total motion decomposes into an exogenous component and a policy-sensitive component,

$$\underbrace{d_t}_{\text{exogenous drift}} + \underbrace{\kappa_t^{(\mathcal{M})}}_{\text{policy-sensitive drift}}, \quad (3)$$

and the resulting budget (2) recovers classical regimes as limiting cases distinguished by which source of motion dominates. In the purely exogenous case $\kappa_t^{(\mathcal{M})} \equiv 0$, the normalized budget C_T/T plays the same operational role as a variation budget *rate*, but is tied to Fisher–Rao motion and to the induced one-step risk shifts rather than imposed in an external discrepancy.

Table 1: Learning regimes recovered as limits of the drift–feedback bound. Each corresponds to nullifying either the exogenous drift d_t or the policy-sensitivity term $\kappa_t^{(\mathcal{M})}$.

Learning regime	Active terms	Representative work	Notes
Stationary <i>i.i.d.</i>	\sqrt{T} term only	Vapnik (1998)	No drift or feedback; fixed $p(x, y)$.
Exogenous drift	d_t term	Besbes et al. (2015)	Distribution changes externally over time.
Performative equilibrium	$d_t \rightarrow 0, \kappa_t^{(\mathcal{M})} \rightarrow 0$	Perdomo et al. (2020)	Coupled learner–environment system converging to a performative equilibrium.
Adaptive data analysis	$\kappa_t^{(\mathcal{M})}$ term	Dwork et al. (2015)	Feedback/adaptivity-driven instability.

A broader online-optimization literature studies nonstationarity via *tracking* objectives and bounds performance through dynamic regret, which scales with the path length of a time-varying comparator sequence and reduces to static regret in the stationary limit (Hall and Willett, 2013; Zhao et al., 2024). These results quantify how well an algorithm can follow a moving target, but they are typically stated in terms of loss-sequence variation or comparator drift and do not address prequential reproducibility gaps induced by *endogenous* distributional evolution. Our analysis

is complementary. It identifies an intrinsic, distribution-level motion rate C_T/T that controls step-to-step population risk shifts along the realized closed-loop trajectory.

Information-theoretic analyses of adaptive learning express related limits in terms of mutual-information accumulation between data and model parameters (Russo and Zou, 2016; Xu and Raginsky, 2017). In statistical physics, learning has been interpreted as a thermodynamic process in which information gain is constrained by entropy production (Still et al., 2012; Goldt and Seifert, 2017; Ortega and Braun, 2013). All of these perspectives describe limited information flow, but they do so with external metrics or equilibrium arguments rather than an intrinsic geometric surrogate tied to Fisher motion.

Finally, the geometric ingredients we use—Fisher information as the canonical invariant metric and the local quadratic expansion of KL—are classical in information geometry (Čencov, 1982; Amari and Nagaoka, 2000; Amari, 2016). A related line of work uses this geometry primarily to motivate *algorithms* (e.g., natural-gradient or Riemannian preconditioning) and adaptive learning dynamics, including in nonstationary or changing environments (Amari et al., 2019; Murata et al., 2002). Our focus is different. Rather than parameter space, we use it to quantify *intrinsic motion of the data-generating law* and to derive nonasymptotic prequential reproducibility limits governed by the drift rate C_T/T , including a matching minimax lower bound. Section 6 further adds an observability principle which isolates what can and cannot be inferred about intrinsic drift from partial observations.

1.4 Contributions and Significance

The proxy budget C_T serves as a *statistical primitive* that provides a tractable accounting of cumulative Fisher–Rao motion in a closed-loop learning process, with operational consequences governed by its *average rate* C_T/T . Where existing theories bound isolated sources of instability (exogenous variation or adaptive feedback), C_T provides a single surrogate that governs both. It reframes prequential reproducibility not as an assumption but as a finite resource whose consumption limits generalization under self-altering dynamics. Building on this primitive, we develop a unified theory of learning under distributional drift in which environmental change and learner feedback jointly shape the data-generating process. The resulting analysis extends stationary learning theory to closed-loop systems and establishes a quantitative limit on how rapidly a learner can adapt, on average, before worst-case prequential reproducibility guarantees become impossible.

The main contributions are:

1. We develop a closed-loop framework for learning under endogenous drift, modeling the data-generating process as a trajectory on a statistical manifold.
2. We define drift primitives $(d_t, \kappa_t^{(\mathcal{M})})$ and a proxy intrinsic drift budget C_T that separates exogenous motion from policy-sensitive motion within Fisher geometry.
3. We establish finite-sample bounds that separate on-trajectory sampling concentration from the drift penalty, yielding explicit contributions from exogenous motion and policy-sensitive feedback and the scaling $\mathbb{E} \Delta_T^{\text{rep}} \lesssim T^{-1/2} + C_T/T$.
4. We prove a matching minimax lower bound on a canonical subclass, establishing that the rate $\Theta(T^{-1/2} + C_T/T)$ is unimprovable for achievable expected generalization error under the drift–feedback model and demonstrating the necessity of the policy-sensitivity term.
5. We show how to obtain an *observable* proxy for drift rate under a fixed monitoring channel: the Fisher–Rao motion of the pushed-forward distributions contracts under the channel and is

therefore uniformly upper-bounded by C_T/T , yielding a practical diagnostic of information drift (and clarifying when observability limits make drift appear artificially small).

6. We validate the theory in three settings: controlled linear–Gaussian drift (where all primitives are closed-form), a nonlinear teacher–learner stress test, and a monitoring-channel experiment that empirically exhibits Fisher contraction and tracks the predicted drift-rate scaling in observable coordinates.

The remainder of the paper is organized as follows. Section 2 introduces preliminary tools used in the analysis; Section 3 formalizes the endogenously drifting process and its metric structure; Section 4 defines the drift measures and intrinsic drift budget; Section 5 presents the main theorems and lower bounds; Section 6 develops observable Fisher–Rao drift rates under monitoring channels; Section 7 reports empirical validation; and Section 8 discusses implications and extensions.

2 Preliminaries and Lemmas

This section collects the technical tools used throughout the paper. We formalize the probabilistic timing and filtration, introduce the Fisher–Rao geometry on the statistical manifold (Θ, g_θ) , and state local regularity assumptions ensuring that distances, logarithm maps, and geodesic comparisons are well behaved along the realized trajectory. We also record the martingale concentration inequality used to control sampling noise (empirical deviation around the realized trajectory risk) and a discrete–continuous identity for Fisher–Rao path length. Full proofs of nonstandard or technically involved statements are deferred to Appendix A.

2.1 Measure–metric foundations

Let \mathcal{H} denote the learner’s hypothesis class, and let $f \in \mathcal{H}$ be a measurable map $\mathcal{X} \rightarrow \mathcal{Y}$ with measurable loss $\ell(f(x), y)$. Let $(\mathcal{X}, \mathcal{Y})$ denote the input–output space with the product σ –algebra, and let $\Theta \subset \mathbb{R}^d$ be a smooth parameter manifold indexing a family of data-generating distributions $\{p_\theta(x, y)\}_{\theta \in \Theta}$. Expectations under p_θ are written $\mathbb{E}_\theta[\cdot]$.

Throughout, expressions of the form $\theta + \Delta\theta$ are understood in a fixed local coordinate chart. When we require an intrinsic tangent displacement between two nearby points $\theta, \theta' \in \Theta$, we write

$$\log_\theta(\theta') \in T_\theta\Theta$$

for the Riemannian logarithm map (defined on the normal neighborhood of θ), so that $\text{Exp}_\theta(\log_\theta(\theta')) = \theta'$.

Definition 2 (Fisher–Rao metric and distance). *For each $\theta \in \Theta$, let $T_\theta\Theta$ denote the tangent space at θ . The Fisher–Rao metric is the Riemannian metric $g_\theta : T_\theta\Theta \times T_\theta\Theta \rightarrow \mathbb{R}$ defined by*

$$g_\theta(v, w) = \mathbb{E}_\theta[\langle \nabla_\theta \log p_\theta(x, y), v \rangle \langle \nabla_\theta \log p_\theta(x, y), w \rangle], \quad v, w \in T_\theta\Theta.$$

In local coordinates $\theta = (\theta^1, \dots, \theta^d)$, with $\partial_i = \partial/\partial\theta^i$, this yields the Fisher information matrix

$$g_{ij}(\theta) = \mathbb{E}_\theta[\partial_i \log p_\theta(x, y) \partial_j \log p_\theta(x, y)].$$

For $v \in T_\theta\Theta$, the induced norm is

$$\|v\|_{g_\theta} = \sqrt{g_\theta(v, v)}.$$

The associated Fisher–Rao geodesic distance between $\theta, \theta' \in \Theta$ is

$$d_F(\theta, \theta') = \inf_{\gamma \in \Gamma(\theta, \theta')} \int_0^1 \|\dot{\gamma}(s)\|_{g_{\gamma(s)}} ds,$$

where $\Gamma(\theta, \theta')$ is the set of piecewise- C^1 curves $\gamma : [0, 1] \rightarrow \Theta$ with $\gamma(0) = \theta$ and $\gamma(1) = \theta'$. See Rao (1945) and Amari and Nagaoka (2000).

2.2 Filtration and sampling semantics

We work with the natural filtration generated by past observations and actions,

$$\mathcal{F}_t = \sigma(x_1, y_1, u_1, \dots, x_t, y_t, u_t).$$

Throughout, the learner may update its predictor and policy using the available history. Concretely, we assume:

1. the environment parameter θ_t is \mathcal{F}_{t-1} -measurable;
2. the predictor f_t and control u_t are \mathcal{F}_{t-1} -measurable (or are drawn from conditional distributions given \mathcal{F}_{t-1}); and
3. conditional on \mathcal{F}_{t-1} , the next observation satisfies $(x_t, y_t) \mid \mathcal{F}_{t-1} \sim p_{\theta_t}$.

Under these conditions,

$$\mathbb{E}[\ell(f_t(x_t), y_t) \mid \mathcal{F}_{t-1}] = \mathbb{E}_{(x,y) \sim p_{\theta_t}}[\ell(f_t(x), y)] =: R(\theta_t, f_t),$$

so the centered loss

$$Z_t := \ell(f_t(x_t), y_t) - R(\theta_t, f_t)$$

is a martingale difference sequence with respect to (\mathcal{F}_t) .

2.3 Regularity and bounded geometry

We impose standing assumptions ensuring that Fisher geometry is well behaved on the region visited by the realized trajectory.

Assumption 1 (Local statistical regularity). *The realized trajectory $\{\theta_t\}_{t=1}^{T+1}$ remains inside a compact set $K \subset \Theta$ on which:*

1. Uniform Fisher regularity. *The Fisher information matrix $g(\theta)$ is finite, positive definite, and smooth on K .*
2. Regular likelihood calculus. *The map $\theta \mapsto \log p_{\theta}(x, y)$ is twice continuously differentiable on a neighborhood of K , and differentiation and integration interchange uniformly on K .*
3. Bounded geometry. *There exists an injectivity radius $r_{\text{inj}} > 0$ such that for all $\theta \in K$, Exp_{θ} is a diffeomorphism on the g_{θ} -ball of radius r_{inj} , and the sectional curvature on K is uniformly bounded.*
4. Sub-Gaussian sampling noise. *The martingale differences Z_t defined above satisfy the conditional sub-Gaussian mgf bound*

$$\mathbb{E}[\exp(\lambda Z_t) \mid \mathcal{F}_{t-1}] \leq \exp\left(\frac{1}{2}\sigma^2\lambda^2\right), \quad \text{for all } \lambda \in \mathbb{R}.$$

Assumption 2 (Local dynamics regularity).

1. Finite-energy actions. *The learner's control inputs satisfy*

$$\mathbb{E}\|u_t\|^2 \leq B, \quad t = 1, \dots, T.$$

2. Local control differentiability of the environment map (chart form). *Fix a local coordinate chart on K . For each $\theta \in K$ and each realized η_t , the environment transition $u \mapsto F(\theta, u, \eta_t)$ is differentiable at $u = 0$ and admits the expansion*

$$F(\theta_t, u_t, \eta_t) = F(\theta_t, 0, \eta_t) + J_u F(\theta_t, 0, \eta_t) u_t + r_t,$$

where r_t is a second-order chart remainder. Moreover, there exists $c > 0$ uniform over $\theta_t \in K$ and admissible u_t such that

$$\|r_t\| \leq c \|u_t\|^2$$

in the chart Euclidean norm. By norm equivalence on compact K , we will always measure this remainder at the baseline next state, so that (possibly with a different constant)

$$\|r_t\|_{g_{F(\theta_t, 0, \eta_t)}} \lesssim \|u_t\|^2.$$

3. Trajectory confinement. *The update $\theta_{t+1} = F(\theta_t, u_t, \eta_t)$ keeps $\theta_{t+1} \in K$ for all t .*

Remark 1 (intrinsic interpretation of the remainder). *When steps remain inside a normal neighborhood, the chart expansion in Assumption 2(2) may be viewed as an intermediate representation of the intrinsic displacement from $F(\theta_t, 0, \eta_t)$ to $F(\theta_t, u_t, \eta_t)$; conversions to Fisher–Rao distance are handled later using local bounded-geometry comparisons along the realized trajectory.*

Lemma 1 (Uniform local KL quadratic bound on K). *Under Assumption 1(1)–(3), there exist constants $\rho \leq r_{\text{inj}}$ and $C_{\text{KL}} < \infty$ such that for all $\theta \in K$ and all $\Delta\theta \in T_\theta\Theta$ with $\|\Delta\theta\|_{g_\theta} \leq \rho$,*

$$D_{\text{KL}}(p_{\text{Exp}_\theta(\Delta\theta)} \| p_\theta) \leq C_{\text{KL}} \|\Delta\theta\|_{g_\theta}^2.$$

Lemma 2 (Local geodesic equivalence). *Let (Θ, g) be a statistical manifold equipped with the Fisher metric, and let $\theta \in K$. If $v \in T_\theta\Theta$ satisfies $\|v\|_{g_\theta} < r_{\text{inj}}$, then the radial geodesic $\gamma(s) = \text{Exp}_\theta(sv)$ is minimizing on $[0, 1]$ and*

$$d_F(\theta, \text{Exp}_\theta(v)) = \|v\|_{g_\theta}. \quad (4)$$

Proof (see Appendix A.1). Since $\|v\|_{g_\theta} \leq r_{\text{inj}}$, the radial geodesic is minimizing on $[0, 1]$. Gauss's lemma implies its length equals $\|v\|_{g_\theta}$, yielding (4); see Lee (1997, Prop. 6.10 and Cor. 6.11). \square

2.4 Concentration tools

Lemma 3 (Sub-Gaussian martingale deviation). *Let $\{Z_t\}_{t=1}^T$ be a martingale difference sequence adapted to $\{\mathcal{F}_t\}$ such that*

$$\mathbb{E}[\exp(\lambda Z_t) \mid \mathcal{F}_{t-1}] \leq \exp\left(\frac{1}{2}\sigma_t^2 \lambda^2\right) \quad \text{for all } \lambda \in \mathbb{R}.$$

Set $S_T = \sum_{t=1}^T Z_t$ and $\mathcal{V}_T = \sum_{t=1}^T \sigma_t^2$. Then for any $\eta > 0$,

$$\Pr(|S_T| \geq \eta) \leq 2 \exp\left(-\frac{\eta^2}{2\mathcal{V}_T}\right).$$

Corollary 1 (Expected deviation). *Under the conditions of Lemma 3,*

$$\mathbb{E}|S_T| \leq \sqrt{2\pi \mathcal{V}_T}, \quad \mathbb{E}\left|\frac{1}{T} \sum_{t=1}^T Z_t\right| \leq \frac{\sqrt{2\pi \mathcal{V}_T}}{T}.$$

In particular, if each Z_t is σ -sub-Gaussian so that $\mathcal{V}_T \leq \sigma^2 T$, then

$$\mathbb{E}\left|\frac{1}{T} \sum_{t=1}^T Z_t\right| \leq \frac{\sqrt{2\pi} \sigma}{\sqrt{T}}.$$

Proof (see Appendix A.2). Integrate the tail bound of Lemma 3:

$$\mathbb{E}|S_T| = \int_0^\infty \Pr(|S_T| \geq \eta) d\eta \leq \int_0^\infty 2 \exp\left(-\frac{\eta^2}{2\mathcal{V}_T}\right) d\eta = \sqrt{2\pi \mathcal{V}_T}.$$

Divide by T for the averaged bound. □

2.5 Length identity for piecewise geodesic interpolation

Lemma 4 (Discrete–continuous Fisher–Rao length identity). *Let $\theta_1, \dots, \theta_{T+1} \in \Theta$ be such that for each $t = 1, \dots, T$ there exists a minimizing Fisher–Rao geodesic connecting θ_t to θ_{t+1} . Let $\gamma_T : [0, 1] \rightarrow \Theta$ be the piecewise C^1 curve obtained by concatenating these minimizing geodesics, parameterized at constant speed on each subinterval $[(t-1)/T, t/T]$ so that $\gamma_T((t-1)/T) = \theta_t$ and $\gamma_T(t/T) = \theta_{t+1}$. Then*

$$\sum_{t=1}^T d_F(\theta_{t+1}, \theta_t) = \int_0^1 \|\dot{\gamma}_T(s)\|_{g_{\gamma_T(s)}} ds, \quad (5)$$

where $\dot{\gamma}_T$ exists for almost every $s \in [0, 1]$.

Proof. For each t , the restriction $\gamma_T|_{[(t-1)/T, t/T]}$ is a constant-speed minimizing geodesic from θ_t to θ_{t+1} . Hence its Riemannian length equals $d_F(\theta_{t+1}, \theta_t)$. Summing over $t = 1, \dots, T$ yields (5). □

Together, Lemmas 2–4 provide the geometric backbone used in Sections 3–5, and Lemma 3 and Corollary 1 provide the concentration backbone used to control the sampling term.

3 Problem Setup

Having established the geometric and concentration tools in Section 2, we now instantiate them in a stochastic process that captures learning under *endogenous drift*—a regime in which the learner’s own actions alter the distribution from which future observations are drawn. Our goal is to express this closed-loop evolution directly in the Fisher geometry defined earlier, so that distributional motion can be quantified in intrinsic terms.

We begin by specifying the coupled learner–environment dynamics introduced in Section 1. As in Section 2, let $(\mathcal{X}, \mathcal{Y})$ denote the input–output space and Θ the parameter manifold indexing the family of distributions $\{p_\theta(x, y)\}_{\theta \in \Theta}$. At each discrete time $t \in \{1, \dots, T\}$,

$$(x_t, y_t) | \mathcal{F}_{t-1} \sim p_{\theta_t}, \quad u_t \sim \pi_t(\mathcal{F}_{t-1}), \quad \theta_{t+1} = F(\theta_t, u_t, \eta_t), \quad (6)$$

where $\mathcal{F}_t = \sigma(x_1, y_1, u_1, \dots, x_t, y_t, u_t)$ is the natural filtration generated by past observations and actions. The map F governs the environment’s evolution, π_t is a (possibly history–dependent) policy, and η_t represents exogenous latent influences. This is the model we analyze here.

Definition 3 (Endogenously Drifting Process). *A learning process $\{(x_t, y_t, \theta_t, u_t)\}_{t=1}^T$ satisfies endogenous drift if the transition $F(\theta_t, u_t, \eta_t)$ depends on the control u_t , thereby coupling the evolution of θ_t to the policy π_t . The variable η_t represents the exogenous influence acting on the environment: a collection of factors, deterministic or stochastic, that evolve independently of u_t and contribute exogenous drift.*

This is the only sense in which we use “endogenous” in what follows.

Example 1 (Linear–Gaussian environment). *A classical linear instance of (6) is*

$$F(\theta_t, u_t, \eta_t) = \theta_t + Au_t + B\eta_t,$$

where A and B determine sensitivity to the learner’s action u_t and to exogenous influences η_t . The term Au_t captures policy-induced motion (vanishing when $A = 0$), while $B\eta_t$ captures background evolution (vanishing when $B = 0$).

This instance satisfies Definition 3 exactly and yields closed-form expressions for Fisher–Rao motion, drift magnitudes $(d_t, \kappa_t^{(\mathcal{M})})$, and the intrinsic budget C_T . It underlies the linear–Gaussian validation in Section 7.

Instantiation (linear regression). *One concrete realization is linear regression with Gaussian covariates $x_t \sim \mathcal{N}(\mu_t, \Sigma)$ and noise $y_t = w^\top x_t + \varepsilon_t$, where $\varepsilon_t \sim \mathcal{N}(0, \sigma^2)$, with environment state $\theta_t = \mu_t$ evolving according to the same map F .*

Endogenous drift thus produces a closed-loop system in which learner and environment co-evolve. If F is independent of u_t , the setting reduces to non-stationary optimization with purely exogenous drift. If F is constant, it reduces to the classical i.i.d. regime. The general case—where both influences are present—yields an evolving distributional flow driven jointly by background change and policy-induced perturbations.

A natural question is whether such coupling might guide the process toward a performative equilibrium, so that policy-induced drift $\kappa_t^{(\mathcal{M})}$ eventually vanishes. In general, this need not occur. The joint evolution of (f_t, θ_t) is not assumed to be a gradient flow on a shared potential, and the environment map F need not be contractive. Even when fixed points exist, stochasticity, misspecification, or misaligned objectives can yield persistent cycles or wandering trajectories. Prior work on performative prediction typically imposes strong stability conditions to study equilibria (Perdomo et al., 2020). Our analysis instead addresses the generic case in which the learner–environment system continues to move along the statistical manifold and the cumulative budget accumulates with T , with prequential step-to-step reproducibility governed by the corresponding rate.

With the dynamics specified, we now express the relevant statistical quantities along the evolving trajectory. The parameter space Θ carries the Fisher–Rao metric g_θ and geodesic distance d_F introduced in Section 2. All norms, distances, and path lengths are understood with respect to this metric, with local equivalence and curvature bounds provided by the regularity conditions. We will keep two distinct effects separate. The first is the usual sampling fluctuation: even if the data-generating law were fixed, the empirical trajectory average need not equal its conditional expectation. The second is geometric: as θ_t moves, the population risk of a *within-step fixed* predictor can change from one step to the next.

We write the empirical trajectory average

$$\widehat{R}_T(f, \pi) = \frac{1}{T} \sum_{t=1}^T \ell(f_t(x_t), y_t), \quad R(\theta, f) := \mathbb{E}_{(x,y) \sim p_\theta}[\ell(f(x), y)].$$

Trajectory (same-time) risk and sampling deviation. The realized-trajectory population risk is

$$R_T^{\text{traj}}(f, \pi) = \frac{1}{T} \sum_{t=1}^T R(\theta_t, f_t) = \frac{1}{T} \sum_{t=1}^T \mathbb{E}_{(x,y) \sim p_{\theta_t}}[\ell(f_t(x), y)].$$

Its sampling deviation is

$$\Delta_T^{\text{sam}}(f, \pi) = |\widehat{R}_T(f, \pi) - R_T^{\text{traj}}(f, \pi)|.$$

Under the filtration conditions stated in Section 2, the centered losses

$$Z_t := \ell(f_t(x_t), y_t) - R(\theta_t, f_t)$$

form a martingale difference sequence, so Δ_T^{sam} is controlled by martingale concentration (as in the stationary case).

Prequential risk and drift penalty. To quantify distributional motion without entangling it with the evolution of f_t , we measure how the population risk of the deployed predictor f_t changes across the environment transition $\theta_t \rightarrow \theta_{t+1}$:

$$\delta_t(f, \pi) := |R(\theta_{t+1}, f_t) - R(\theta_t, f_t)|.$$

Its time average

$$V_T(f, \pi) := \frac{1}{T} \sum_{t=1}^T \delta_t(f, \pi)$$

isolates the effect of environment motion: if $\theta_{t+1} = \theta_t$ then $V_T(f, \pi) = 0$ regardless of how (f_t) evolves.

The prequential (one-step-ahead) population risk is

$$R_T^+(f, \pi) := \frac{1}{T} \sum_{t=1}^T R(\theta_{t+1}, f_t),$$

and we define the corresponding prequential gap

$$\Delta_T^{\text{rep}}(f, \pi) := |\widehat{R}_T(f, \pi) - R_T^+(f, \pi)|.$$

An add-subtract decomposition yields the full separation

$$\Delta_T^{\text{rep}}(f, \pi) \leq \underbrace{\left| \frac{1}{T} \sum_{t=1}^T (\ell(f_t(x_t), y_t) - R(\theta_t, f_t)) \right|}_{\Delta_T^{\text{sam}}(f, \pi)} + \underbrace{\frac{1}{T} \sum_{t=1}^T |R(\theta_{t+1}, f_t) - R(\theta_t, f_t)|}_{V_T(f, \pi)}.$$

Equivalently,

$$\Delta_T^{\text{rep}}(f, \pi) \leq \Delta_T^{\text{sam}}(f, \pi) + V_T(f, \pi). \quad (7)$$

Thus sampling noise contributes the classical $T^{-1/2}$ term, while drift enters only through the geometric penalty V_T , which will be controlled by Fisher–Rao motion along the realized trajectory.

Equation (7) also clarifies why standard average loss curves can be misleading in closed loop. Because Δ_T^{rep} is a *trajectory-average* gap, it can remain small even when substantial drift occurs, so long as the resulting risk shifts do not register as persistent average discrepancy. By contrast, V_T records the *within-step* population-risk change of a fixed predictor across each transition $\theta_t \rightarrow \theta_{t+1}$, and therefore isolates drift effects that may be invisible in aggregate averages. The subsequent analysis relates this drift penalty to intrinsic Fisher motion along the trajectory (via C_T), and Section 5 formalizes the associated speed-limit regime by matching upper and minimax lower bounds.

Remark 2 (Bounded geometry as a learnability regime). *Equation (7) separates sampling fluctuation from the drift penalty V_T , but it does not by itself guarantee that V_T is small. The role of the Fisher–Rao framework is to identify regimes in which V_T can be controlled by intrinsic motion along the realized trajectory. If the coupled dynamics induce sufficiently “wild” motion that the process leaves the bounded-geometry regime, then the statistical geometry no longer provides uniform control of risk variation, and no general prequential reproducibility guarantee should be expected. The confinement conditions in Section 2 therefore function as a learnability condition for closed-loop reproducibility.*

The drift primitives $(d_t, \kappa_t^{(\mathcal{M})})$ and the budget C_T are chosen precisely so that Fisher–Rao motion controls V_T . We therefore describe the environment’s motion on (Θ, g_θ) by separating an exogenous baseline step from a policy-sensitive perturbation.

Exogenous drift. The exogenous drift magnitude is

$$d_t := d_F(F(\theta_t, 0, \eta_t), \theta_t),$$

capturing the motion that would occur at time t in the absence of control.

To reduce clutter we suppress η_t in expressions where it plays no structural role in the drift decomposition, writing $F(\theta_t, u_t) \equiv F(\theta_t, u_t, \eta_t)$ and $F(\theta_t, 0) \equiv F(\theta_t, 0, \eta_t)$ when the dependence is clear from context.

Policy-sensitive drift. Policy-sensitive drift is measured by the leading-order Fisher–metric motion induced by the learner’s action. Under Assumption 2, the map $u \mapsto F(\theta_t, u, \eta_t)$ is differentiable at $u = 0$, so

$$F(\theta_t, u_t, \eta_t) = F(\theta_t, 0, \eta_t) + J_u F(\theta_t, 0, \eta_t) u_t + r_t,$$

with a quadratic remainder. The differential $J_u F(\theta_t, 0, \eta_t) u_t$ is a tangent vector at the baseline next state $F(\theta_t, 0, \eta_t)$, and we define

$$\kappa_t^{(\mathcal{M})} := \|J_u F(\theta_t, 0, \eta_t) u_t\|_{g_F(\theta_t, 0, \eta_t)}. \quad (8)$$

We will use this linearization in Section 4 to compare $\kappa_t^{(\mathcal{M})}$ to intrinsic Fisher–Rao displacements up to a second-order remainder.

These components combine to form the intrinsic drift budget

$$C_T = \sum_{t=1}^T (d_t + \alpha \kappa_t^{(\mathcal{M})}),$$

a tractable surrogate for the intrinsic Fisher–Rao path length \mathcal{A}_T . The scalar $\alpha > 0$ is not a model parameter. It is a fixed weighting that sets the relative contribution of policy-sensitive motion to the budget C_T . It may also absorb constants from local comparison inequalities (under the bounded-geometry regime on K) that relate the linearized control displacement $J_u F(\theta_t, 0, \eta_t) u_t$ to the corresponding Fisher–Rao displacement.

The update (6) defines a trajectory on (Θ, g_θ) . The quantities d_t and $\kappa_t^{(\mathcal{M})}$ describe its incremental motion, while C_T records the accumulated proxy budget for this motion. Together, d_t , $\kappa_t^{(\mathcal{M})}$, and C_T serve as the geometric primitives of the framework and anchor the drift–feedback bounds developed in Section 5.

4 Quantifying Drift and Feedback

The quantities introduced in Section 3 describe the instantaneous motion of the data-generating process on the statistical manifold (Θ, g_θ) . This section shows how these local motions accumulate over time and yields the drift–feedback budget whose normalized rate C_T/T controls two intrinsic quantities along the realized trajectory: (i) the Fisher–Rao path length traveled by the environment and (ii) the trajectory-averaged population-risk variation. Combined with the sampling decomposition developed later, these controls lead to the prequential reproducibility bounds in Section 5.2.

4.1 Drift Decomposition

Since F is smooth in the control variable (Assumption 2), we can expand the update in a fixed local coordinate chart $\Theta \subset \mathbb{R}^d$:

$$\theta_{t+1} = F(\theta_t, 0, \eta_t) + J_u F(\theta_t, 0, \eta_t) u_t + r_t, \quad (9)$$

where r_t collects higher-order terms. The role of (9) is purely *comparative*: it is a coordinate representation used to control intrinsic Fisher–Rao distances on the compact region K visited by the realized trajectory. We do not identify chart differences with intrinsic displacements beyond uniform constant-factor bounds.

To isolate the genuinely second-order contribution, define

$$\epsilon_t := \|r_t\|_{g_{F(\theta_t, 0, \eta_t)}}.$$

By Assumption 2(2), the remainder is pointwise quadratic, so

$$\epsilon_t \leq c \|u_t\|^2. \quad (10)$$

The intrinsic one-step motion is measured by the Fisher–Rao distance $d_F(\theta_{t+1}, \theta_t)$. We first split this motion into a baseline (exogenous) step and a policy-sensitive perturbation using the triangle inequality:

$$d_F(\theta_{t+1}, \theta_t) \leq d_F(\theta_{t+1}, F(\theta_t, 0, \eta_t)) + d_F(F(\theta_t, 0, \eta_t), \theta_t). \quad (11)$$

The second term is exactly the exogenous drift distance; recalling the definition from Section 3,

$$d_t := d_F(F(\theta_t, 0, \eta_t), \theta_t).$$

The first term requires a comparison between the linearized control displacement and intrinsic

Fisher–Rao distance. We assume a local comparison on K , valid for example in a small–step regime where the controlled perturbation remains inside a uniform normal neighborhood. There exists a constant $\alpha > 0$ such that

$$d_F(\theta_{t+1}, F(\theta_t, 0, \eta_t)) \leq \alpha \kappa_t^{(\mathcal{M})} + \epsilon_t, \quad (12)$$

where $\kappa_t^{(\mathcal{M})}$ is the policy–sensitive drift magnitude from Section 3, and ϵ_t is the second-order remainder from (10). The constant α collects the uniform local equivalence constants between the linearized control displacement and Fisher–Rao distance on K .

Combining (11) and (12) yields:

$$d_F(\theta_{t+1}, \theta_t) \leq d_t + \alpha \kappa_t^{(\mathcal{M})} + \epsilon_t. \quad (13)$$

Equation (13) expresses intrinsic motion as the sum of the exogenous step, the policy sensitive contribution, and a second-order residual. The residual is isolated in ϵ_t and controlled by (10).

4.2 Cumulative Motion Rate and the Intrinsic Drift Budget

Accumulating intrinsic one–step distances yields the discrete Fisher–Rao path length

$$\mathcal{A}_T = \sum_{t=1}^T d_F(\theta_{t+1}, \theta_t). \quad (14)$$

Summing over t gives

$$\mathcal{A}_T \leq \sum_{t=1}^T (d_t + \alpha \kappa_t^{(\mathcal{M})} + \epsilon_t) = C_T + \sum_{t=1}^T \epsilon_t. \quad (15)$$

Recalling the intrinsic drift budget

$$C_T = \sum_{t=1}^T (d_t + \alpha \kappa_t^{(\mathcal{M})}),$$

C_T upper-bounds the realized Fisher–Rao path length up to the quadratic residual $\sum_{t=1}^T \epsilon_t$, which is upper-bounded by control energy via (10). In regimes where this remainder is small (e.g., small control), C_T serves as a tractable surrogate for total Fisher–Rao motion.

4.3 From Geometric Motion to Risk Variation

We now relate Fisher–Rao motion to variation in population risk. On the regularity region K , we assume the population risk is Lipschitz in Fisher–Rao distance. Lemma 5 in Section 5.2 gives a convenient sufficient condition under which this Lipschitz-in-Fisher property holds.

Assumption 3 (Risk regularity on K). *There exists $L_p < \infty$ such that for all $\theta, \theta' \in K$ and all measurable predictors f considered by the learner,*

$$|R(\theta', f) - R(\theta, f)| \leq L_p d_F(\theta', \theta),$$

where $R(\theta, f)$ is the population risk defined in Section 3.

Applying Assumption 3 with $(\theta, \theta') = (\theta_t, \theta_{t+1})$ gives

$$|R(\theta_{t+1}, f_t) - R(\theta_t, f_t)| \leq L_p d_F(\theta_{t+1}, \theta_t). \quad (16)$$

Combining (16) with the one-step motion bound (13) yields the pathwise risk-variation control

$$|R(\theta_{t+1}, f_t) - R(\theta_t, f_t)| \leq L_p d_t + L_p \alpha \kappa_t^{(\mathcal{M})} + L_p \epsilon_t. \quad (17)$$

Using (10), the residual term is controlled by control energy, so there exist constants $C_1, C_2, C_3 > 0$ (depending only on L_p, α , and the remainder constant c in Assumption 2(2), (up to norm equivalence on K) such that

$$|R(\theta_{t+1}, f_t) - R(\theta_t, f_t)| \leq C_1 d_t + C_2 \kappa_t^{(\mathcal{M})} + C_3 \|u_t\|^2. \quad (18)$$

We now record the two ingredients needed for the main prequential reproducibility bound in Section 5. The first is a martingale control of the sampling deviation Δ_T^{sam} around the realized trajectory risk R_T^{traj} . The second is a geometric control of the drift penalty V_T , obtained by summing the pathwise risk-variation bound (17).

For reference, we write the trajectory risk variation in the explicit predictor-fixed form

$$V_T(f, \pi) := \frac{1}{T} \sum_{t=1}^T |R(\theta_{t+1}, f_t) - R(\theta_t, f_t)|. \quad (19)$$

The bound (17) is the key step: it converts geometric motion into one-step population-risk change. In Section 5 we sum this inequality and combine it with (7) to obtain the prequential reproducibility law.

5 Theoretical Results

The geometric structure introduced above yields sharp limits for learning under the endogenous drift model ((6)). We control Δ_T^{sam} by martingale concentration and we bound V_T by Fisher–Rao motion, relating it to the proxy intrinsic drift budget C_T . This yields a prequential reproducibility bound of order $T^{-1/2} + C_T/T$. A matching lower bound on a canonical subclass shows that this scaling cannot be improved in general.

Throughout this section, all expectations, suprema, and minimax statements are taken over the class of drift–feedback processes generated by Assumptions 1–2 and the transition model $\theta_{t+1} = F(\theta_t, u_t, \eta_t)$ in (6), with arbitrary learning rules (f_t) and policies (π_t) . All full proofs are provided in Appendix A.

5.1 Local Fisher–Risk Coupling

Let the population loss of the current learner f_t under environment parameter θ be

$$\mathcal{L}_t(\theta) = \mathbb{E}_{(x,y) \sim p_\theta} [\ell(f_t(x), y)].$$

Smoothness of the risk functional implies that Fisher–Rao motion controls variation in population risk, but this requires a *uniform-in- θ* regularity condition. We therefore separate two distinct roles: (i) the trajectory-conditional sub-Gaussian assumption used for sampling concentration (Assumption 1(4)), and (ii) a uniform Fisher–risk regularity condition used to convert Fisher motion into risk variation.

Lemma 5 gives a convenient sufficient condition under which Assumption 3 holds (with an explicit constant).

Lemma 5 (Local Fisher–Risk Coupling). *Fix t and write $\mathcal{L}_t(\theta) = \mathbb{E}_{p_\theta}[\ell(f_t(x), y)]$. Assume that for this t the centered loss*

$$\tilde{Z}_{\theta,t}(x, y) := \ell(f_t(x), y) - \mathcal{L}_t(\theta)$$

is uniformly σ -sub-Gaussian under p_θ over $\theta \in K$, i.e.,

$$\sup_{\theta \in K} \mathbb{E}_{p_\theta} \left[\exp(\lambda \tilde{Z}_{\theta,t}(x, y)) \right] \leq \exp\left(\frac{1}{2}\sigma^2 \lambda^2\right) \quad \text{for all } \lambda \in \mathbb{R}.$$

Then Assumption 3 holds for this t with $L_p = \sqrt{c_{\text{sg}}}\sigma$, where c_{sg} is the universal constant relating sub-Gaussian tails to second moments under the adopted convention.

Proof. Let $\gamma : [0, 1] \rightarrow K$ be a constant-speed Fisher geodesic from θ to θ' , and define $g(s) = \mathcal{L}_t(\gamma(s))$. Differentiating under the integral sign (justified by Assumption 1) yields

$$g'(s) = \mathbb{E}_{(x,y) \sim p_{\gamma(s)}} \left[\ell(f_t(x), y) \langle s_{\gamma(s)}(x, y), \dot{\gamma}(s) \rangle \right],$$

where $s_\vartheta = \nabla_\vartheta \log p_\vartheta$ is the score. Using $\mathbb{E}_{p_\vartheta}[s_\vartheta] = 0$ and centering the loss gives

$$g'(s) = \mathbb{E}_{p_{\gamma(s)}} \left[\tilde{Z}_{\gamma(s),t}(x, y) \langle s_{\gamma(s)}(x, y), \dot{\gamma}(s) \rangle \right].$$

By Cauchy–Schwarz and the definition of the Fisher metric,

$$|g'(s)| \leq \sqrt{\mathbb{E}_{p_{\gamma(s)}} \left[\tilde{Z}_{\gamma(s),t}^2 \right]} \|\dot{\gamma}(s)\|_{g_{\gamma(s)}}.$$

The uniform σ -sub-Gaussian assumption implies $\mathbb{E}_{p_{\gamma(s)}} \left[\tilde{Z}_{\gamma(s),t}^2 \right] \leq c_{\text{sg}}\sigma^2$, uniformly in s . Hence $|g'(s)| \leq \sqrt{c_{\text{sg}}}\sigma \|\dot{\gamma}(s)\|_{g_{\gamma(s)}}$. Integrating along γ yields

$$|\mathcal{L}_t(\theta') - \mathcal{L}_t(\theta)| \leq \sqrt{c_{\text{sg}}}\sigma \int_0^1 \|\dot{\gamma}(s)\|_{g_{\gamma(s)}} ds = \sqrt{c_{\text{sg}}}\sigma d_F(\theta', \theta),$$

which is exactly Assumption 3 with $L_p = \sqrt{c_{\text{sg}}}\sigma$. \square

Interpretation. Lemma 5 is the bridge from geometry to risk: a uniform moment envelope on the centered loss makes $\mathcal{L}_t(\theta)$ Lipschitz in Fisher–Rao distance on K . We use it only to turn motion bounds into control of V_T ; it is not a stability or speed-limit assumption.

5.2 Drift–Feedback Bounds

We now bound the prequential gap Δ_T^{rep} by assembling the decomposition (7), martingale concentration for the sampling term, and Fisher–Rao motion control for the drift penalty V_T .

Lemma 6 (Summed drift penalty). *Let V_T be as in (19). Under Assumption 3,*

$$V_T(f, \pi) \leq \frac{L_p}{T} \left(C_T + \sum_{t=1}^T \epsilon_t \right), \quad (20)$$

where ϵ_t is the remainder from (10). Consequently, using (10),

$$V_T(f, \pi) \leq \frac{L_p}{T} C_T + \frac{L_p c}{T} \sum_{t=1}^T \|u_t\|^2.$$

Proof (See Appendix A.4). By (16) and (13), $|R(\theta_{t+1}, f_t) - R(\theta_t, f_t)| \leq L_p(d_t + \alpha \kappa_t^{(\mathcal{M})} + \epsilon_t)$. Sum over t and divide by T to obtain (20), then apply (10). \square

Lemma 7 (Collected bounds). *Under the endogenous–drift model (6) and Assumptions 1 and 3, for any learner (f, π) ,*

$$\mathbb{E} \Delta_T^{\text{sam}}(f, \pi) \leq \frac{\sqrt{2\pi} \sigma}{\sqrt{T}}, \quad \mathbb{E} V_T(f, \pi) \leq \frac{L_p}{T} \mathbb{E}[C_T] + \frac{L_p c}{T} \sum_{t=1}^T \mathbb{E} \|u_t\|^2.$$

Proof. For the sampling term, $Z_t = \ell(f_t(x_t), y_t) - R(\theta_t, f_t)$ is a martingale difference sequence under (6), so Corollary 1 gives $\mathbb{E} \Delta_T^{\text{sam}} \leq \sqrt{2\pi} \sigma / \sqrt{T}$. For the drift term, apply Lemma 6 and take expectations. \square

Theorem 1 (Prequential reproducibility under drift). *Under the endogenous–drift model (6), Assumptions 1 and 3, for any learner (f, π) ,*

$$\mathbb{E} \Delta_T^{\text{rep}}(f, \pi) \leq \frac{\sqrt{2\pi} \sigma}{\sqrt{T}} + \frac{L_p}{T} \mathbb{E}[C_T] + \frac{L_p c}{T} \sum_{t=1}^T \mathbb{E} \|u_t\|^2.$$

Proof (See Appendix A.5). We start from the pathwise decomposition (7):

$$\Delta_T^{\text{rep}}(f, \pi) \leq \Delta_T^{\text{sam}}(f, \pi) + V_T(f, \pi).$$

Taking expectations yields

$$\mathbb{E} \Delta_T^{\text{rep}}(f, \pi) \leq \mathbb{E} \Delta_T^{\text{sam}}(f, \pi) + \mathbb{E} V_T(f, \pi). \quad (21)$$

Define $Z_t := \ell(f_t(x_t), y_t) - R(\theta_t, f_t)$. Under (6), $\{Z_t\}_{t=1}^T$ is a martingale difference sequence: $\mathbb{E}[Z_t \mid \mathcal{F}_{t-1}] = 0$. Assumption 1(4) gives the conditional σ -sub-Gaussian mgf bound. Hence Corollary 1 yields

$$\mathbb{E} \Delta_T^{\text{sam}}(f, \pi) = \mathbb{E} \left| \frac{1}{T} \sum_{t=1}^T Z_t \right| \leq \frac{\sqrt{2\pi} \sigma}{\sqrt{T}}.$$

By Lemma 6 and (10),

$$V_T(f, \pi) \leq \frac{L_p}{T} C_T + \frac{L_p c}{T} \sum_{t=1}^T \|u_t\|^2.$$

Taking expectations yields

$$\mathbb{E} V_T(f, \pi) \leq \frac{L_p}{T} \mathbb{E}[C_T] + \frac{L_p c}{T} \sum_{t=1}^T \mathbb{E} \|u_t\|^2.$$

Substituting the two displays into (21) yields the theorem. \square

The final term is a second–order energy remainder. In small–step regimes it is dominated by the linear budget term $\mathbb{E}[C_T]/T$. In particular, on any class where $C_T \leq C$ almost surely and $\sum_{t=1}^T \mathbb{E} \|u_t\|^2 = O(1)$, the drift contribution reduces to $O(C/T)$.

Interpretation. Theorem 1 separates the prequential gap into a classical sampling term scaling as $T^{-1/2}$ and a drift penalty controlled (up to a second-order remainder) by the average intrinsic budget C_T/T . Thus, when $C_T \ll \sqrt{T}$ the prequential error is sampling-dominated, while for $C_T \gg \sqrt{T}$ the geometric motion of the data-generating process dominates.

5.3 Lower Bound and Speed Limit

We now show that the scaling in Theorem 1 is tight on a canonical subclass. The key tension in any drift-dependent lower bound is that the construction must (i) keep candidate processes statistically hard to tell apart (small KL divergence), while (ii) forcing enough cumulative Fisher–Rao motion to make their drift-induced trajectory variation genuinely differ. Our construction uses many *short Fisher geodesic excursions* that return to a common base point: KL accumulates quadratically in excursion size, while Fisher path length (and the induced risk variation) accumulates linearly. The construction exploits the KL Fisher quadratic expansion: KL accumulates quadratically while Fisher arc length accumulates linearly, forcing an unavoidable C/T drift penalty.

Theorem 2 (Lower Bound). *There exists a subclass \mathcal{P}_C of drift-feedback processes satisfying Assumptions 1–2 and $\mathbb{E}_P[C_T] \leq C$ such that, with $R_T^+(P) := \frac{1}{T} \sum_{t=1}^T R(\theta_{t+1}, f_t)$,*

$$\inf_{\hat{R}_T} \sup_{P \in \mathcal{P}_C} \mathbb{E}_P |\hat{R}_T - R_T^+(P)| \geq c_1 \max\left(T^{-1/2}, \frac{C}{T}\right),$$

for a constant $c_1 > 0$ depending only on fixed model constants and α .

Proof (see Appendix A.6). We define \mathcal{P}_C by an explicit one-dimensional exponential-family model and a family of deterministic drift trajectories indexed by a codebook.

Model and geometry. Fix a one-dimensional regular exponential family $\{p_\theta\}$ on a compact interval where Fisher information is bounded above and below, and reparameterize into Fisher arclength coordinates so that $d_F(\theta, \theta') = |\theta - \theta'|$ on this interval (cf. Amari and Nagaoka, 2000). Consider controllable dynamics

$$F(\theta_t, u_t, \eta_t) = \theta_t + u_t, \quad \eta_t \equiv 0,$$

so $d_t \equiv 0$, $J_u F \equiv 1$, and the remainder term vanishes. In this subclass $\kappa_t^{(\mathcal{M})} = |u_t|$ and $C_T = \alpha \sum_{t=1}^T |u_t|$.

Excursions and budget. Fix a step size $\delta > 0$ and partition the horizon into m disjoint two-step blocks. For a sign vector $v \in \{-1, +1\}^m$, define a history-independent policy that in block j applies $u = v_j \delta$ and then $u = -v_j \delta$, returning to the base point after two steps. The resulting parameter path executes m geodesic excursions of length 2δ , hence

$$C_T(P_v) = \alpha \sum_{t=1}^T |u_t| = 2\alpha m \delta.$$

Choose

$$m = \left\lfloor \frac{C}{2\alpha\delta} \right\rfloor \wedge \left\lfloor \frac{T}{2} \right\rfloor,$$

so $C_T(P_v) \leq C$ for all v (in fact C_T is deterministic here).

Risk separation. Fix a bounded loss/model pair and fix a (history-independent) learner sequence (f_t) for which the population risk has a nonzero local slope at the base point θ_0 on the indices used

in the construction: there exists $c_0 > 0$ such that for all sufficiently small δ ,

$$|R(\theta_0 + \delta, f_{2j-1}) - R(\theta_0 - \delta, f_{2j-1})| \geq c_0 \delta, \quad j = 1, \dots, m.$$

If v and w differ in $\Omega(m)$ blocks, then on the corresponding excursions their one-step-ahead states $\theta_{2j}^{(v)}$ and $\theta_{2j}^{(w)}$ differ by 2δ on $\Omega(m)$ indices, forcing

$$|R_T^+(P_v) - R_T^+(P_w)| \gtrsim \frac{m\delta}{T} = \frac{1}{T} \left(\left\lfloor \frac{C}{2\alpha\delta} \right\rfloor \wedge \left\lfloor \frac{T}{2} \right\rfloor \right) \delta \asymp \min\left(\frac{C}{T}, \delta\right), \quad R_T^+(P) := \frac{1}{T} \sum_{t=1}^T R(\theta_{t+1}, f_t).$$

In particular, choosing δ so that $\lfloor C/(2\alpha\delta) \rfloor \leq \lfloor T/2 \rfloor$ yields separation $\gtrsim C/T$.

KL control and Fano. Because the trajectories are deterministic and the observations are conditionally independent given θ_t , the joint law factorizes and

$$D_{\text{KL}}(P_v \| P_w) = \sum_{t=1}^T D_{\text{KL}}(p_{\theta_t^{(v)}} \| p_{\theta_t^{(w)}}).$$

The trajectories differ only on the indices in disagreeing blocks. On a compact interval, regular exponential families satisfy a uniform local quadratic KL bound 1, so each disagreeing block contributes $O(\delta^2)$ KL on the step where the parameters differ. Thus $D_{\text{KL}}(P_v \| P_w) \lesssim m\delta^2$. Choose a binary codebook $V \subset \{-1, +1\}^m$ with $|V| \geq 2^{\Omega(m)}$ and minimum Hamming distance $\Omega(m)$ (Tsybakov and Zaiats, 2009, Lemma 2.9). Taking δ small enough so that the resulting family $\{P_v\}_{v \in V}$ satisfies a standard Fano-type testing condition, the usual testing-to estimation reduction yields a minimax lower bound of order $m\delta/T \asymp C/T$ for estimating $R_T^+(P)$ over \mathcal{P}_C (see Tsybakov and Zaiats (2009, Sec. 2.2–2.3); cf. Yu (1997)). Restricting to the stationary subclass ($C_T = 0$) recovers the classical $\Omega(T^{-1/2})$ term, giving the combined $\max(T^{-1/2}, C/T)$ rate. \square

Interpretation. Theorem 2 shows that feedback-driven drift imposes an *irreducible* prequential penalty in a minimax sense. Even when trajectories remain within a small Fisher neighborhood, an information motion budget $\mathbb{E}_P[C_T] \leq C$ yields an $\Omega(C/T)$ lower bound on the worst-case expected prequential error (equivalently, on estimating R_T^+) over \mathcal{P}_C .

Corollary 2 (Prequential Speed Limit (tightness on a subclass)). *For the subclass \mathcal{P}_C from Theorem 2,*

$$\inf_{\widehat{R}_T} \sup_{P \in \mathcal{P}_C} \mathbb{E}_P |\widehat{R}_T - R_T^+(P)| = \Theta\left(T^{-1/2} + \frac{C}{T}\right),$$

with constants depending only on fixed model constants and α .

Interpretation. Together with the upper bound in Theorem 1, this yields the tight minimax rate on \mathcal{P}_C . Corollary 2 formalizes a prequential reproducibility speed limit on this canonical drift-feedback subclass: the worst-case achievable expected prequential error over \mathcal{P}_C scales as $\Theta\left(T^{-1/2} + \frac{C}{T}\right)$, so in the drift-dominated regime $C/T \gg T^{-1/2}$, no method can achieve expected estimation error $o(C/T)$ uniformly over \mathcal{P}_C .

Alternative estimands on the same realized path. The preceding bounds control drift through intrinsic motion of the realized trajectory, summarized by \mathcal{A}_T and the proxy budget C_T (hence the rate C_T/T). This machinery applies to other drift functionals defined on the *same* path. For example, fixing a reference predictor f_{ref} (e.g., a frozen f_0 or benchmark f^*), define

$$V_T^{\text{ref}} := \frac{1}{T} \sum_{t=1}^T |R(\theta_{t+1}, f_{\text{ref}}) - R(\theta_t, f_{\text{ref}})|.$$

Under Assumption 3, one has $V_T^{\text{ref}} \leq \frac{L_p}{T} \sum_{t=1}^T d_F(\theta_{t+1}, \theta_t) = \frac{L_p}{T} \mathcal{A}_T \lesssim \frac{L_p}{T} (C_T + \sum_{t=1}^T \epsilon_t)$. The difference from V_T is the estimand (risk is evaluated at f_{ref} rather than the deployed f_t), not the geometric control, which depends only on the realized motion. Hence, the same techniques applied here may be used on a variety of drift problems.

5.4 Stationary and Classical Limits

Our results recover standard learning regimes as special cases of $(d_t, \kappa_t^{(\mathcal{M})})$ by nullifying one or both components of geometric motion. We emphasize the separation established above. Sampling deviation around the realized trajectory risk is controlled at the classical $T^{-1/2}$ rate, while drift enters the prequential gap through the penalty term V_T in $\Delta_T^{\text{rep}} \leq \Delta_T^{\text{sam}} + V_T$.

- **i.i.d. regime.** If $d_t \equiv 0$ and $J_u F \equiv 0$ (so $\theta_{t+1} = \theta_t$), then the environment does not move and $V_T(f, \pi) = 0$ and $\Delta_T^{\text{rep}}(f, \pi) = \Delta_T^{\text{sam}}(f, \pi)$, giving $\mathbb{E} \Delta_T^{\text{rep}}(f, \pi) = O(T^{-1/2})$, matching classical results (Vapnik, 1998).
- **Exogenous drift.** If $J_u F \equiv 0$ but $d_t > 0$, then $\kappa_t^{(\mathcal{M})} \equiv 0$ and Lemma 7 yields $\mathbb{E} V_T(f, \pi) \lesssim (1/T) \sum_t \mathbb{E}[d_t]$, which is directly analogous in form to variation–budget penalties in nonstationary optimization (Besbes et al., 2015).
- **Performative equilibrium.** If both drift components vanish asymptotically (so $d_t \rightarrow 0$ and $\kappa_t^{(\mathcal{M})} \rightarrow 0$), then $\mathbb{E} V_T(f, \pi) \rightarrow 0$ and the only remaining contribution is sampling deviation at rate $T^{-1/2}$. This corresponds to regimes where the coupled learner–environment system stabilizes, as in performative equilibrium analyses (Perdomo et al., 2020).
- **Feedback-driven drift.** If $d_t \equiv 0$ but $\kappa_t^{(\mathcal{M})} > 0$, then $\mathbb{E} V_T(f, \pi) \lesssim (1/T) \sum_t \mathbb{E}[\kappa_t^{(\mathcal{M})}]$. This captures purely policy-induced instability of the data-generating process and is conceptually aligned with feedback effects studied in adaptive data analysis, though the mechanism here is an evolving population law rather than a fixed database (Dwork et al., 2015; Russo and Zou, 2016; Bassily et al., 2016).

Formally, these regimes correspond to projections of the same geometric decomposition onto axes of the drift vector $(d_t, \kappa_t^{(\mathcal{M})})$. Setting one component to zero restricts the intrinsic drift budget $C_T = \sum_t (d_t + \alpha \kappa_t^{(\mathcal{M})})$ to the remaining axis and yields the corresponding specialization of the stability bound.

Taken together, these results identify a geometric quantity that governs learning under drift. The intrinsic drift budget C_T upper bounds the total Fisher–Rao motion of the coupled learner–environment system and controls drift-induced instability through the scaling $O(C_T/T)$, while sampling deviation retains the classical $O(T^{-1/2})$ rate.

5.5 Practical implications

A cautionary point in drift–feedback systems is that the realized loss trajectory is not, by itself, a certificate of prequential optimality. The same observed losses can be compatible with qualitatively different regimes: one in which the learner is near the best attainable one-step-ahead performance for the realized environment, and one in which there remains substantial avoidable excess risk. What separates these regimes is not a particular adaptation heuristic, but the *information speed* of the realized environment trajectory. Our bounds therefore single out the average drift rate C_T/T as the quantity governing how accurately one-step-ahead performance can be certified from the data stream.

A simple toy construction makes the point. Consider squared loss with a one-dimensional environment parameter $\theta_t = A(-1)^t$ and a sequence of predictions a_t . Compare two predictors without committing to a learning rule: the lagged predictor $a_t = \theta_{t-1}$ and the time-average baseline $a_t \equiv 0$. Their losses differ by a constant factor. The lagged predictor incurs $(a_t - \theta_t)^2 = 4A^2$ at every step, whereas the baseline incurs A^2 . The catch is that the lagged predictor cannot diagnose from its realized losses alone whether it is limited by the information available or instead being defeated by a structured, high-rate trajectory that makes one-step extrapolation systematically wrong. The ambiguity is about identifiability of the regime, not about the form of the update.

This is exactly the role played by the rate C_T/T in the theory. It distinguishes regimes in which prequential performance is estimation-limited from those in which it is drift-limited. When the realized motion rate is small, additional data and improved estimation can reduce one-step-ahead error. When the motion rate is nonnegligible, there is an irreducible floor on certifying step-ahead performance that does not vanish with T ; in that regime, the observed loss need not reflect how close one is to the best achievable prequential risk along the realized trajectory.

Finally, in feedback settings the *composition* of the motion matters as well as its magnitude. Our decomposition separates exogenous Fisher motion $d_t = d_F(\theta_{t+1}^{\text{exo}}, \theta_t)$ from the policy-induced increment $\kappa_t^{(\mathcal{M})} = d_F(\theta_{t+1}, \theta_{t+1}^{\text{exo}})$, so that $C_T = \sum_{t=1}^T (d_t + \alpha \kappa_t^{(\mathcal{M})})$. Even coarse information about how much of the realized drift rate is self-induced changes what can be inferred from observed losses. When exogenous motion dominates, large prequential error is plausibly attributed to a fast-moving target. When endogenous motion dominates, the same error can reflect amplification through the drift–feedback loop. This distinction is precisely what d_t and $\kappa_t^{(\mathcal{M})}$ formalize, and it clarifies why loss-only monitoring cannot, in general, resolve regime without some accompanying drift-rate signal.

6 Observable Fisher Motion

Our analysis above is phrased in intrinsic terms. The realized Fisher–Rao motion

$$\mathcal{A}_T = \sum_{t=1}^T d_F(p_{\theta_{t+1}}, p_{\theta_t})$$

is the path length of the realized environment trajectory on the statistical manifold of data-generating laws, and the drift budget C_T provides a tractable surrogate that upper-bounds this motion up to the second-order remainder isolated in Section 4. These quantities are appealing precisely because they are intrinsic to the family $\{p_\theta\}_{\theta \in \Theta}$ and do not depend on a particular coordinate choice for θ . At the same time, they are defined at the level of the full law p_{θ_t} , whereas an adaptive system typically observes only a coarsened view of each sample.

To connect intrinsic drift to what can be monitored, fix a time-homogeneous Markov kernel K from the data space to an observation space \mathcal{O} . It may represent a deterministic statistic $o = \psi(z)$,

a randomized coarsening (e.g., quantization with noise), or more generally any fixed measurable channel producing an observed representation of z . Applying K to a law p produces the pushforward distribution $K_{\#}p$ on \mathcal{O} ,

$$(K_{\#}p)(A) = \int K(A | z)p(dz), \quad A \subseteq \mathcal{O} \text{ measurable.}$$

Given the family $\{p_{\theta}\}$, the channel induces a corresponding family on \mathcal{O} via $q_{\theta} := K_{\#}p_{\theta}$. We may therefore speak of Fisher–Rao geometry not only for the intrinsic law but also for its channel image.

A key fact is that Fisher geometry is monotone under such channels. In Čencov’s characterization, Fisher information is the unique Riemannian metric that is invariant under sufficient statistics and, more generally, contracts under Markov morphisms (Čencov, 1982; Amari and Nagaoka, 2000). In the present setting, this yields a concrete contraction statement for Fisher–Rao distances.

Proposition 3 (Fisher–Rao contraction under Markov kernels). *Let $\{p_{\theta}\}_{\theta \in \Theta}$ be a regular statistical family equipped with Fisher information metric and associated geodesic distance d_F . Let K be a time-homogeneous Markov kernel mapping the data space to \mathcal{O} , and define $q_{\theta} := K_{\#}p_{\theta}$. Equip $\{q_{\theta}\}$ with its Fisher–Rao geodesic distance. Then for all $\theta, \theta' \in \Theta$,*

$$d_F(q_{\theta}, q_{\theta'}) \leq d_F(p_{\theta}, p_{\theta'}). \quad (22)$$

Consequently, for any realized trajectory $\theta_1, \dots, \theta_{T+1}$,

$$\sum_{t=1}^T d_F(q_{\theta_{t+1}}, q_{\theta_t}) \leq \sum_{t=1}^T d_F(p_{\theta_{t+1}}, p_{\theta_t}) = \mathcal{A}_T. \quad (23)$$

Proof. Monotonicity of the Fisher information metric under Markov morphisms (Čencov, 1982; Amari and Nagaoka, 2000) implies that the tangent map induced by $p \mapsto K_{\#}p$ contracts Fisher norms. Writing $g^{(p)}$ and $g^{(q)}$ for the Fisher information metrics on $\{p_{\theta}\}$ and $\{q_{\theta}\}$, respectively, for any tangent vector v at p_{θ} ,

$$\|K_{\#}v\|_{g_{\theta}^{(q)}} \leq \|v\|_{g_{\theta}^{(p)}}.$$

Therefore, the Fisher–Rao length of any smooth curve in Θ cannot increase after applying $K_{\#}(\cdot)$. Applying this to a minimizing Fisher–Rao geodesic between θ and θ' yields (22). Summing along the realized trajectory gives (23). \square

Proposition 3 turns a fixed observation channel into an intrinsic quantity on the output space. Along the trajectory, define $q_t := K_{\#}p_{\theta_t}$ and the observed Fisher motion

$$\mathcal{A}_T^{(K)} = \sum_{t=1}^T d_F(q_{t+1}, q_t), \quad \text{with observed Fisher rate } \mathcal{A}_T^{(K)}/T.$$

This quantity depends only on what is visible through \mathcal{O} . It is computable when the induced family is tractable, and it is estimable from windowed samples when \mathcal{O} is low-dimensional or well-approximated by a simple parametric family. The guarantee is not that $\mathcal{A}_T^{(K)}/T$ recovers the intrinsic drift rate, but that it is the canonical Fisher-rate associated with the chosen channel, and that it can only decrease as observation becomes coarser.

Combining Proposition 3 with the intrinsic bound $\mathcal{A}_T \leq C_T + \sum_t \epsilon_t$ yields an immediate link between observable rates and the drift budget.

Corollary 3 (Observed Fisher motion is bounded by the intrinsic drift budget). *Fix a Markov kernel K and define $q_t := K_{\#}p_{\theta_t}$ along the trajectory. Let*

$$\mathcal{A}_T^{(K)} := \sum_{t=1}^T d_F(q_{t+1}, q_t).$$

Then $\mathcal{A}_T^{(K)} \leq \mathcal{A}_T$. Moreover, under the drift–feedback decomposition of Section 4,

$$\frac{\mathcal{A}_T^{(K)}}{T} \leq \frac{\mathcal{A}_T}{T} \leq \frac{C_T}{T} + \frac{1}{T} \sum_{t=1}^T \epsilon_t, \quad (24)$$

where C_T is the intrinsic drift budget and ϵ_t is the second-order remainder term from (13)–(15).

Proof. The inequality $\mathcal{A}_T^{(K)} \leq \mathcal{A}_T$ follows from (23). The bound on \mathcal{A}_T is (15). Dividing by T gives (24). \square

The content of Corollary 3 is straightforward. Any fixed channel induces an information speed on its output space. This speed is measured in Fisher units, is additive over time, and is dominated by the intrinsic drift rate up to the second-order term. A large observed Fisher rate therefore certifies that the realized trajectory is not moving slowly in intrinsic geometry, whereas a small observed rate indicates only that the chosen channel does not reveal substantial Fisher motion on the timescale being monitored.

Finally, our emphasis on Fisher–Rao motion should not be read as a rejection of drift diagnostics based on standard divergences. Many monitoring approaches quantify change via KL (or related divergences) between successive windows of model outputs, learned representations, or other summary statistics. The present theory helps explain why such measures can be informative. When changes are incremental, KL admits a local quadratic approximation governed by Fisher information, so rates of per-step divergence can track changes in the operative information drift regime. For example, one may consider a distance-like cumulative score of the form

$$\hat{\mathcal{A}}_T^{(\text{KL})} = \sum_{t=1}^{T-1} \sqrt{2 \hat{D}_{\text{KL}}(Q_{t+1} \parallel Q_t)},$$

which is locally calibrated to Fisher motion up to second-order terms. At the same time, this connection is representation-dependent. Under any fixed coarse-graining the induced divergences can only decrease, so an observed divergence that remains small may reflect limited sensitivity of the monitored representation rather than genuine stationarity.

7 Experimental Validation

This section validates the two empirical quantities that organize our theory—the prequential gap and its decomposition into sampling and drift—and the observed Fisher motion under monitoring channels. We start in a linear–Gaussian environment where all terms are available in closed form. We then move to a nonlinear teacher–learner system with closed-loop feedback and ask whether the same additive structure continues to organize Δ_T^{rep} beyond the analytically tractable regime. Finally, we illustrate the observable Fisher motion and its relationship to the intrinsic drift budget.

7.1 Linear–Gaussian demonstration: budgeted drift component and horizon scaling

We include a closed–form Gaussian model to instantiate the primitives appearing in the decomposition. We consider Gaussian mean estimation with fixed covariance Σ and a drifting environment state $\theta_t \in \mathbb{R}^d$. At time t we observe $x_t \sim \mathcal{N}(\theta_t, \Sigma)$ and deploy the predictor $f_t = \hat{\mu}_{t-1}$, where $\hat{\mu}_t$ is the online sample mean.

Our target quantity is the one–step–ahead prequential gap $\Delta_T^{\text{rep}} = |\widehat{R}_T - R_T^+|$, together with the decomposition $\Delta_T^{\text{rep}} \leq \Delta_T^{\text{sam}} + V_T$ from Section 3. In this setting the population risk is $R(\theta, f) = \text{tr}(\Sigma) + \|\theta - f\|_2^2$, so the above terms can be computed exactly. In this model, nothing is hidden.

Budgeted scaling of the drift component. To isolate the drift contribution, we examine how V_T scales with the Fisher–consistent motion budget. The environment evolves via an exogenous Fisher–budgeted increment plus an endogenous feedback component, yielding four regimes (iid, exogenous only, endogenous only, mixed). For each run we record

$$\bar{d}_T := \frac{1}{T} \sum_{t=1}^T \|v_t^{\text{exo}}\|_{\Sigma^{-1}}, \quad \bar{\kappa}_T := \frac{1}{T} \sum_{t=1}^T \|\gamma u_t\|_{\Sigma^{-1}}, \quad \frac{C_T}{T} := \bar{d}_T + \alpha \bar{\kappa}_T,$$

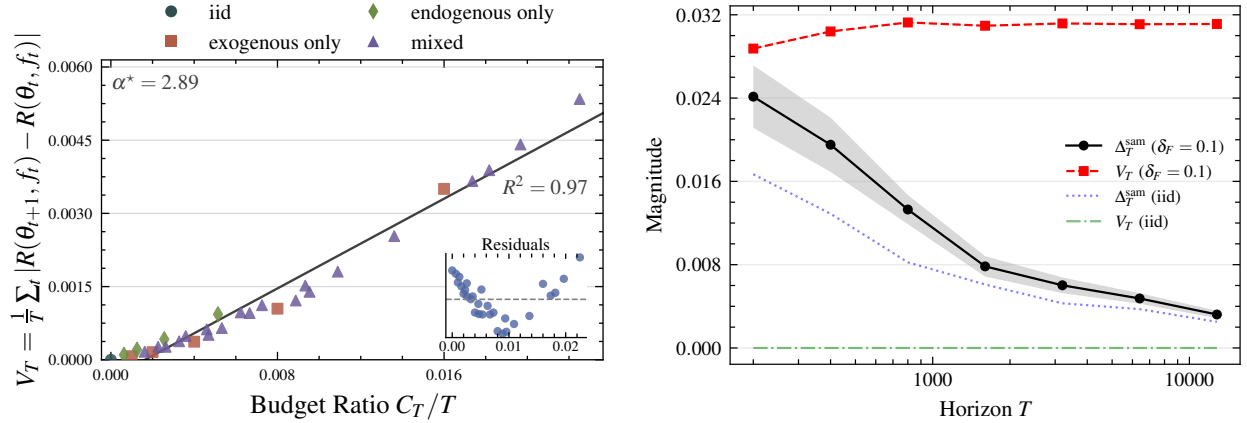
and fit α^* by linear regression. This a key check for the theoretical results. Figure 3(a) shows a tight collapse of V_T as an approximately linear function of C_T/T across regimes (fit: $\alpha^* \approx 2.89$, $R^2 \approx 0.97$), confirming the predicted additivity of exogenous and feedback contributions in this closed–form regime.

Horizon scaling of sampling vs. drift. We next illustrate how the decomposition separates horizon effects. Fixing a persistent bounded drift level (here $\delta_F = 0.1$), we plot the empirical sampling term Δ_T^{sam} together with V_T as functions of T . Figure 3(b) shows that Δ_T^{sam} decreases with T , whereas V_T remains approximately stable, so the dominant contribution transitions from sampling–driven to drift–driven as the horizon grows.

7.2 Nonlinear neural-network validation: teacher–learner drift

We test the same structure in a nonlinear teacher–learner environment in which the learner is trained online and the environment state evolves through closed-loop feedback. At time t , covariates are sampled as $x_t \sim \mathcal{N}(0, I_d)$ and the teacher generates labels $y_t = \langle \phi(x_t), \theta_t \rangle + \varepsilon_t$ with $\varepsilon_t \sim \mathcal{N}(0, \sigma^2)$, where ϕ is a fixed nonlinear feature map and $\theta_t \in \mathbb{R}^m$ is the environment state. The learner is a two-layer MLP f_t updated by streaming SGD on (x_t, y_t) . The environment update combines an exogenous Fisher–budgeted increment with an endogenous component that moves θ_t along a clipped disagreement-gradient direction between student predictions and the teacher rule. We report results over 12 seeds with horizons $T \in \{800, 1600, 3200, 6400\}$, exogenous ratios $C_{\text{exo}}/T \in \{2.5, 5, 10, 20, 40, 80\} \times 10^{-3}$, and feedback strengths $\gamma \in \{0, 0.0025, 0.005, 0.01, 0.02\}$, using input dimension $d = 5$, feature dimension $m = 64$ (i.e., $\phi : \mathbb{R}^d \rightarrow \mathbb{R}^m$), hidden width 128, and noise level $\sigma = 0.1$.

Evaluation. Population MSE $R(\theta, f)$ is approximated by Monte Carlo evaluation on fresh draws from the teacher distribution. When evaluation is subsampled along a nonstationary trajectory, \widehat{R}_T



(a) Drift component V_T vs. budget ratio C_T/T (fit gives $\alpha^* \approx 2.89$, $R^2 \approx 0.97$). (b) Component scaling vs. horizon T : Δ_T^{sam} decays while V_T is approximately constant (illustrated at $\delta_F = 0.1$ with iid reference).

Figure 3: Linear-Gaussian demonstrations for the decomposition $\Delta_T^{\text{rep}} \leq \Delta_T^{\text{sam}} + V_T$. (a) The drift component V_T scales linearly with the Fisher-consistent budget ratio C_T/T across iid, exogenous, endogenous, and mixed regimes. (b) As T increases, the sampling term decreases while the drift component remains stable, illustrating the separation of sampling and drift effects.

and R_T^+ must be computed on a common evaluation schedule; we enforce this by recording both quantities at identical evaluation times (including $t = T$).

Ablation across horizons. Figure 4 (left) plots Δ_T^{rep} versus C_{exo}/T for each horizon, with separate curves for γ . Across horizons, Δ_T^{rep} increases with C_{exo}/T , and larger γ generally yields a larger gap at fixed C_{exo}/T . Thus the feedback channel acts as an additional source of distributional motion that can amplify the prequential gap in this nonlinear closed-loop setting.

Budget collapse with held-out horizon. We form the combined proxy

$$\frac{C_T}{T} := \frac{\sum_{t=1}^T d_t + \alpha \sum_{t=1}^T \kappa_t}{T},$$

and estimate α by fitting the additivity plane

$$\Delta_T^{\text{rep}} \approx b_0 + b_s T^{-1/2} + b_1 \left(\frac{\sum_t d_t}{T} \right) + b_2 \left(\frac{\sum_t \kappa_t}{T} \right)$$

on all horizons except a held-out $T_{\text{hold}} = 6400$, setting $\alpha = b_2/b_1$. In this experiment the fit yields $\alpha \simeq 3.85$ and achieves $R^2 \simeq 0.78$ for the plane model on Δ_T^{rep} . Figure 4 (right) then plots Δ_T^{rep} versus C_T/T within each horizon using this single value of α , including the held-out $T = 6400$ panel. The within-horizon relationships are well-approximated by a linear dependence on C_T/T , supporting the predicted additive organization of Δ_T^{rep} by the combined Fisher-motion budget.

Observed vs. predicted. Figure 5 plots observed Δ_T^{rep} against the corresponding plane predictions from the fit trained on $T \neq T_{\text{hold}}$. The concentration of points near the diagonal, including the

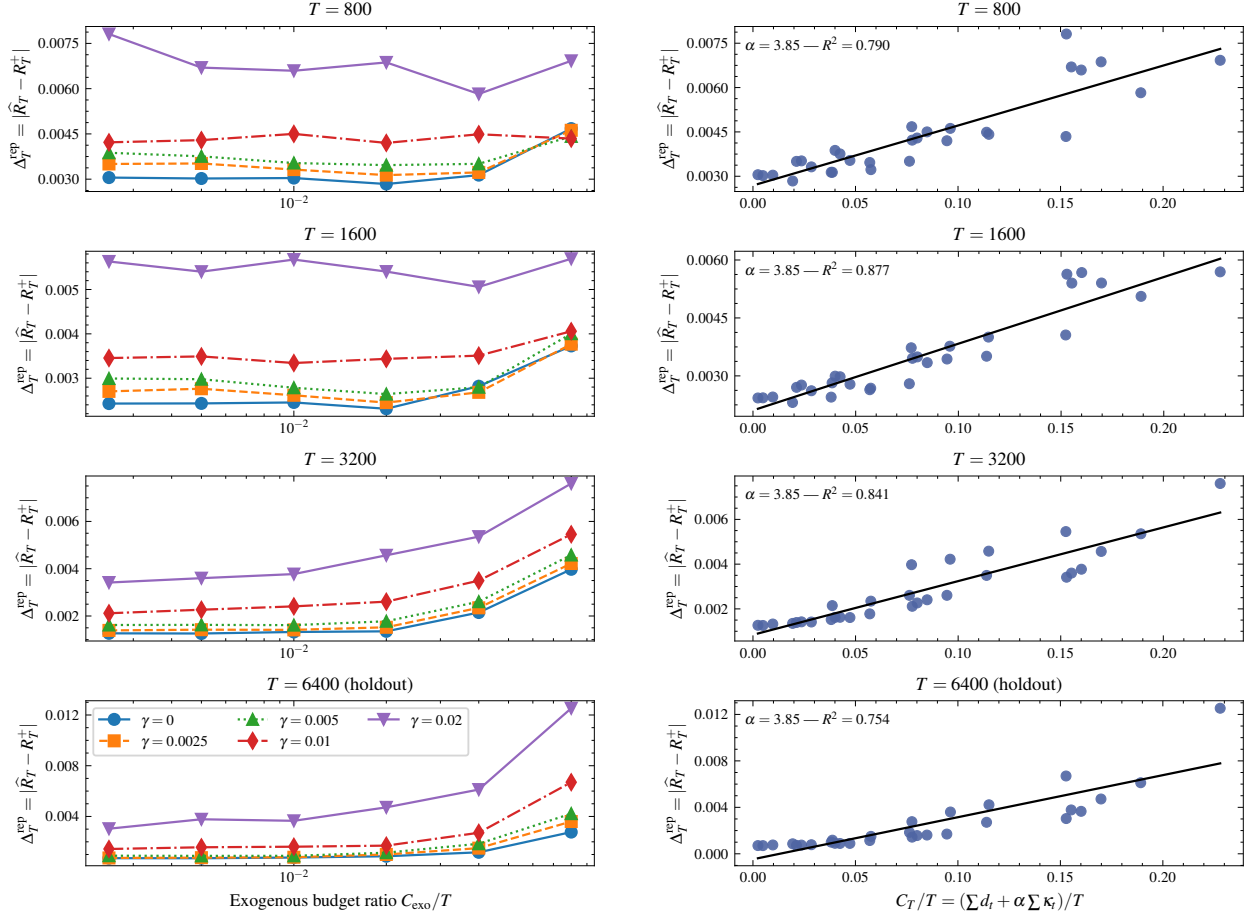


Figure 4: Neural-network teacher–learner validation. *Left*: $\Delta_T^{\text{rep}} = |\widehat{R}_T - R_T^+|$ versus the exogenous ratio C_{exo}/T for horizons $T \in \{800, 1600, 3200, 6400\}$ and feedback strengths γ . *Right*: Within-horizon collapse versus $C_T/T = (\sum_t d_t + \alpha \sum_t \kappa_t)/T$, where α is fitted on $T \neq 6400$ and evaluated on the held-out horizon.

held-out horizon, shows that the plane fit captures most of the dependence of Δ_T^{rep} on $T^{-1/2}$ and the two budget components, including the held-out horizon.

7.3 Observable Fisher Motion under Monitoring Channels

This experiment illustrates the monotonicity bridge in Section 6 in a setting where both the intrinsic Fisher–Rao motion and its channel-induced counterpart are available in closed form. We consider the linear–Gaussian location model $P_t = \mathcal{N}(\theta_t, \Sigma)$ (with fixed Σ), evolving under the same mixed exogenous/endogenous drift–feedback dynamics used throughout our Gaussian validation experiment. As in Section 6, the intrinsic one-step Fisher–Rao distance admits a closed form,

$$d_F(P_{t+1}, P_t) = \|\theta_{t+1} - \theta_t\|_{\Sigma^{-1}}, \quad \mathcal{A}_T(P) = \sum_{t=1}^T d_F(P_{t+1}, P_t).$$

To model an *observable monitoring channel*, we fix a time-homogeneous linear Gaussian kernel K of the form

$$o = Bx + \xi, \quad \xi \sim \mathcal{N}(0, \sigma_K^2 I_k),$$

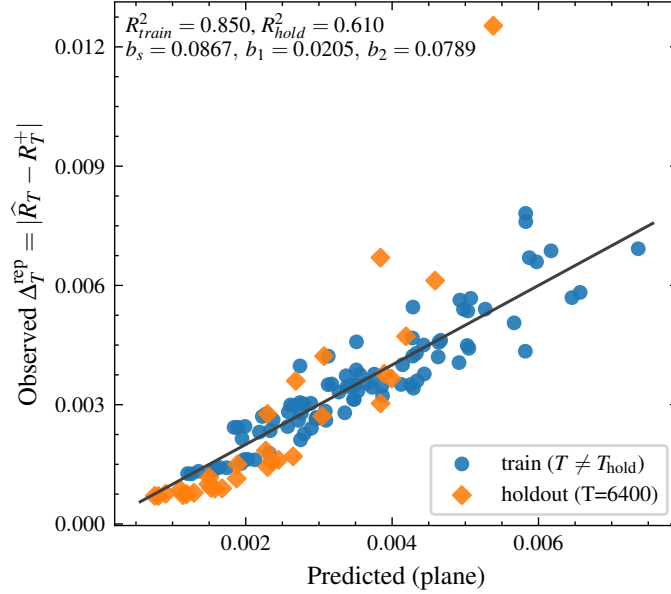


Figure 5: Observed Δ_T^{rep} versus predictions from the plane fit trained on $T \neq T_{\text{hold}}$ (with $T_{\text{hold}} = 6400$ highlighted).

where $B \in \mathbb{R}^{k \times d}$ is a fixed random projection (row-normalized) and $\sigma_K > 0$ is channel noise. The induced output law $Q_t := K_{\#} P_t$ remains Gaussian, $Q_t = \mathcal{N}(B\theta_t, B\Sigma B^\top + \sigma_K^2 I_k)$, and therefore its Fisher–Rao step length is again closed form:

$$d_F(Q_{t+1}, Q_t) = \|B(\theta_{t+1} - \theta_t)\|_{(B\Sigma B^\top + \sigma_K^2 I_k)^{-1}}, \quad \mathcal{A}_T^{(K)} = \sum_{t=1}^T d_F(Q_{t+1}, Q_t).$$

We report the *local Fisher rate* by a trailing-window average, $\bar{a}_t(P) := \frac{1}{|\mathcal{W}_t|} \sum_{s \in \mathcal{W}_t} d_F(P_{s+1}, P_s)$ (and analogously $\bar{a}_t^{(K)}$ for Q_t), which makes regime changes in drift speed visible. To stress the rate interpretation, we allocate the same total exogenous budget across time in bursts (piecewise-constant weights with fixed mean), so that the intrinsic rate alternates between low- and high-speed intervals while keeping C_{exo} fixed.

Figure 6 shows two complementary views. The right panel verifies the stepwise contraction $d_F(Q_{t+1}, Q_t) \leq d_F(P_{t+1}, P_t)$ for each of three monitoring channels, matching Proposition 3. The left panel plots the corresponding local rates. Across all bursts, the induced observed rates track the same temporal structure as the intrinsic rate but remain uniformly smaller, with stronger coarsening (smaller k , larger σ_K) producing a more severe contraction. In the run shown, the average intrinsic Fisher rate is $\mathcal{A}_T(P)/T = 1.105 \times 10^{-3}$, while the observed rates are reduced by factors ≈ 0.76 , 0.55 , and 0.33 for the three channels, respectively.

8 Discussion and Outlook

The preceding analysis identifies the intrinsic drift budget C_T as a statistical primitive for closed-loop learning under distributional drift. It yields a simple organizing consequence: prequential reproducibility is governed by the *average* motion rate C_T/T , which separates estimation limited regimes (sampling-dominated) from drift-limited regimes (with persistent error floors). In this

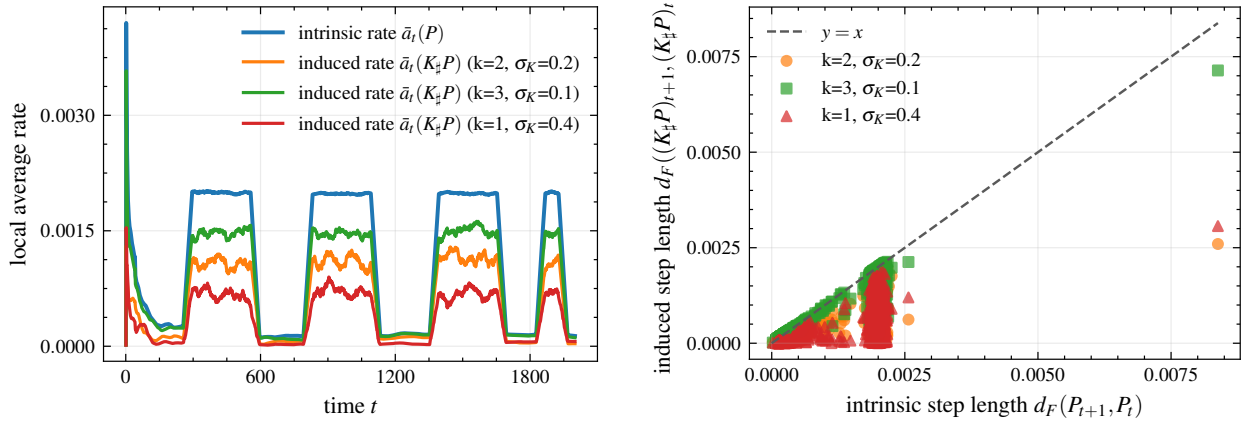


Figure 6: Observable Fisher motion under a fixed monitoring channel K in a linear–Gaussian drift–feedback system. *Left*: local Fisher rate $\bar{a}_t(P)$ (intrinsic) and the induced rates $\bar{a}_t^{(K)}$ on three channel outputs $Q_t = K_{\#}P_t$. Exogenous drift is scheduled in bursts (fixed total budget) to highlight time-varying speed. *Right*: stepwise contraction $d_F(Q_{t+1}, Q_t) \leq d_F(P_{t+1}, P_t)$, illustrating monotonicity of Fisher–Rao distance under Markov kernels.

sense, C_T/T acts as a prequential speed limit. That rate is what matters. Once the realized drift rate is nonnegligible, worst-case statistical self-consistency guarantees become impossible to maintain uniformly. The Fisher–Rao formulation provides an intrinsic sense of motion for the environment-indexed family $\{p_{\theta}\}$, and its additivity over steps is what makes a cumulative budget, and hence a rate, meaningful.

In practice, the transition law $F(\theta_t, u_t, \eta_t)$ is rarely known in full, and the intrinsic quantities $(d_t, \kappa_t^{(\mathcal{M})})$ are not directly observable. Section 6 therefore shifts attention from estimating C_T to monitoring *observable Fisher motion* under a fixed channel. If $q_t = K_{\#}p_{\theta_t}$ denotes the pushed-forward distribution induced by a monitoring kernel K , then the channel motion $\mathcal{A}_T^{(K)} = \sum_{t=1}^{T-1} d_F(q_{t+1}, q_t)$ contracts relative to intrinsic motion and is uniformly controlled by the intrinsic drift rate. The monitoring-channel experiment in Section 7 empirically exhibits this contraction and shows that a trailing-window estimate of $\mathcal{A}_T^{(K)}/T$ can track changes in drift rate even when the underlying trajectory is only partially observed. At the same time, contraction makes an important limitation explicit: small observed motion can reflect an uninformative channel rather than genuine stability.

Several limitations suggest directions for extension. Our results require only local regularity along the realized trajectory (in particular, confinement to a bounded-geometry region and a small-control expansion of the transition in the u variable) rather than a globally specified dynamics. Stochasticity is already permitted through the perturbations η_t , and history dependence can be absorbed into an enlarged state when a Markov representation is available. The substantive restriction is that our drift control proceeds through local Fisher geometry and a Fisher–risk regularity condition, which may fail under abrupt regime changes, discontinuities, or trajectories that leave the regular region. On the observability side, Section 6 treats fixed monitoring channels. A concrete direction is to characterize which classes of channels yield observed motion rates $\mathcal{A}_T^{(K)}/T$ that remain sensitive to the intrinsic rate, and to diagnose “blind” representations for which drift is systematically hidden by contraction.

More broadly, the results suggest that prequential reproducibility is not merely an experimental property but a *resource*: a finite amount of geometric motion that adaptive systems must expend.

Algorithms differ not only in how they optimize an objective but also in how quickly they consume this budget along their trajectories. Understanding how to measure, allocate, or conserve this budget may offer a design principle for learning systems that remain reliable under evolving data sources.

Classical generalization theory often relies on quantities that are not exactly computable for modern models—Rademacher complexities, stability coefficients, and PAC–Bayesian divergences among them. Their value lies in isolating the structural invariant that governs generalization, even when only coarse empirical access is available. The intrinsic drift budget plays the same role for drift–feedback systems. It identifies the geometric quantity that determines when statistical self-consistency can or cannot be maintained, operationally through the drift-rate control C_T/T . Ultimately, C_T offers a way to reason about learning dynamics that is orthogonal to both optimization and statistical complexity, capturing the intrinsic cost of interacting with a changing world.

Declarations

Funding. No external funding supported this work.

Conflict of interest. The author declares no competing interests.

Code availability. Source code and figure-generation scripts for all experiments are available at <https://github.com/fiazaich/Learning-under-Drift>.

A Proofs

For completeness we include proofs of the primary lemmas, theorems and equations. Throughout, constants may depend on the regularity and bounded-geometry constants from Assumption 1, but not on T or on particular parameter values within compact subsets of Θ .

A.1 Proof of Lemma 2 (Local geodesic equivalence)

Proof. Fix $\theta \in K$ and let $v \in T_\theta\Theta$ satisfy $\|v\|_{g_\theta} \leq r_{\text{inj}}$. Let

$$\gamma : [0, 1] \rightarrow \Theta, \quad \gamma(s) := \text{Exp}_\theta(sv).$$

Then γ is a geodesic with $\gamma(0) = \theta$ and $\gamma(1) = \text{Exp}_\theta(v)$ by definition of the exponential map.

Minimizing property inside the injectivity radius. By the definition of the injectivity radius at θ , the restriction of the exponential map Exp_θ to the open ball $B_{r_{\text{inj}}}(0) \subset T_\theta\Theta$ is a diffeomorphism onto its image, and every point in $\text{Exp}_\theta(B_{r_{\text{inj}}}(0))$ is joined to θ by a *unique* minimizing geodesic (see, e.g., standard consequences of the injectivity-radius definition; cf. Lee (1997, Prop. 6.10)). Since $\|v\|_{g_\theta} \leq r_{\text{inj}}$, the endpoint $\text{Exp}_\theta(v)$ lies in this normal neighborhood, hence γ is the (unique) minimizing geodesic from θ to $\text{Exp}_\theta(v)$ on $[0, 1]$. In particular,

$$d_F(\theta, \text{Exp}_\theta(v)) = L(\gamma),$$

where $L(\gamma)$ denotes the Riemannian length of γ .

Constant speed and length computation. Because γ is a geodesic, its speed is constant: $s \mapsto \|\dot{\gamma}(s)\|_{g_{\gamma(s)}}$ is constant on $[0, 1]$. Moreover, $\dot{\gamma}(0) = v$ (differentiate $\text{Exp}_\theta(sv)$ at $s = 0$), so the

constant speed equals $\|v\|_{g_\theta}$:

$$\|\dot{\gamma}(s)\|_{g_{\gamma(s)}} = \|\dot{\gamma}(0)\|_{g_\theta} = \|v\|_{g_\theta} \quad \text{for all } s \in [0, 1].$$

Therefore the length is

$$L(\gamma) = \int_0^1 \|\dot{\gamma}(s)\|_{g_{\gamma(s)}} ds = \int_0^1 \|v\|_{g_\theta} ds = \|v\|_{g_\theta}.$$

Combining the minimizing property with the length computation yields

$$d_F(\theta, \text{Exp}_\theta(v)) = L(\gamma) = \|v\|_{g_\theta},$$

which is exactly (4). □

A.2 Proofs of Lemma 3 and Corollary 1 (Sub-Gaussian martingale deviation and expected deviation)

The following is a standard Chernoff/mgf argument for martingale differences; we include it for completeness (see Wainwright (2019, Section 2.2.2))

Proof of Lemma 3. Let $\{Z_t\}_{t=1}^T$ be a martingale difference sequence adapted to $\{\mathcal{F}_t\}$ and assume that for all $\lambda \in \mathbb{R}$,

$$\mathbb{E}[\exp(\lambda Z_t) \mid \mathcal{F}_{t-1}] \leq \exp\left(\frac{1}{2}\sigma_t^2 \lambda^2\right).$$

Define $S_t := \sum_{s=1}^t Z_s$ with $S_0 := 0$, and $\mathcal{V}_t := \sum_{s=1}^t \sigma_s^2$.

MGF bound for the partial sums. We claim that for all $t \in \{0, 1, \dots, T\}$ and all $\lambda \in \mathbb{R}$,

$$\mathbb{E}[\exp(\lambda S_t)] \leq \exp\left(\frac{1}{2}\lambda^2 \mathcal{V}_t\right). \tag{25}$$

The case $t = 0$ is immediate since $S_0 = 0$ and $\mathcal{V}_0 = 0$. For the inductive step, write

$$\mathbb{E}[\exp(\lambda S_t)] = \mathbb{E}[\exp(\lambda S_{t-1}) \exp(\lambda Z_t)] = \mathbb{E}[\exp(\lambda S_{t-1}) \mathbb{E}[\exp(\lambda Z_t) \mid \mathcal{F}_{t-1}]],$$

where we used that S_{t-1} is \mathcal{F}_{t-1} -measurable. Applying the conditional sub-Gaussian bound yields

$$\mathbb{E}[\exp(\lambda S_t)] \leq \mathbb{E}\left[\exp(\lambda S_{t-1}) \exp\left(\frac{1}{2}\sigma_t^2 \lambda^2\right)\right] = \exp\left(\frac{1}{2}\sigma_t^2 \lambda^2\right) \mathbb{E}[\exp(\lambda S_{t-1})].$$

Invoking the induction hypothesis for $t - 1$ gives

$$\mathbb{E}[\exp(\lambda S_t)] \leq \exp\left(\frac{1}{2}\sigma_t^2 \lambda^2\right) \exp\left(\frac{1}{2}\lambda^2 \mathcal{V}_{t-1}\right) = \exp\left(\frac{1}{2}\lambda^2 \mathcal{V}_t\right),$$

which establishes (25).

One-sided tail bound. Fix $\eta > 0$ and $\lambda > 0$. By Markov's inequality and (25) with $t = T$,

$$\Pr(S_T \geq \eta) = \Pr(\exp(\lambda S_T) \geq \exp(\lambda \eta)) \leq \exp(-\lambda \eta) \mathbb{E}[\exp(\lambda S_T)] \leq \exp\left(-\lambda \eta + \frac{1}{2}\lambda^2 \mathcal{V}_T\right).$$

Optimizing the right-hand side over $\lambda > 0$ gives the minimizer $\lambda^* = \eta/\mathcal{V}_T$ and hence

$$\Pr(S_T \geq \eta) \leq \exp\left(-\frac{\eta^2}{2\mathcal{V}_T}\right).$$

Applying the same argument to $-S_T$ yields $\Pr(S_T \leq -\eta) \leq \exp(-\eta^2/(2\mathcal{V}_T))$. Therefore,

$$\Pr(|S_T| \geq \eta) \leq \Pr(S_T \geq \eta) + \Pr(S_T \leq -\eta) \leq 2 \exp\left(-\frac{\eta^2}{2\mathcal{V}_T}\right),$$

as claimed. □

Proof of Corollary 1. By the tail integral identity for nonnegative random variables,

$$\mathbb{E}|S_T| = \int_0^\infty \Pr(|S_T| \geq \eta) d\eta.$$

Applying Lemma 3 gives

$$\mathbb{E}|S_T| \leq \int_0^\infty 2 \exp\left(-\frac{\eta^2}{2\mathcal{V}_T}\right) d\eta.$$

Using the Gaussian integral $\int_0^\infty \exp(-\eta^2/(2\mathcal{V}_T)) d\eta = \sqrt{\pi\mathcal{V}_T}/2$ yields

$$\mathbb{E}|S_T| \leq \sqrt{2\pi\mathcal{V}_T}.$$

Dividing by T gives

$$\mathbb{E}\left|\frac{1}{T} \sum_{t=1}^T Z_t\right| = \frac{1}{T} \mathbb{E}|S_T| \leq \frac{\sqrt{2\pi\mathcal{V}_T}}{T}.$$

If in addition each Z_t is σ -sub-Gaussian so that $\sigma_t^2 \leq \sigma^2$ and hence $\mathcal{V}_T = \sum_{t=1}^T \sigma_t^2 \leq \sigma^2 T$, then

$$\mathbb{E}\left|\frac{1}{T} \sum_{t=1}^T Z_t\right| \leq \frac{\sqrt{2\pi\sigma^2 T}}{T} = \frac{\sqrt{2\pi}\sigma}{\sqrt{T}}.$$

□

A.3 Proof of Equation 15 (Information path bound)

Proof. Recall the discrete Fisher–Rao path length

$$\mathcal{A}_T := \sum_{t=1}^T d_F(\theta_{t+1}, \theta_t).$$

Work pathwise.

Triangle split into exogenous and controlled components. For each t , insert the baseline next state $F(\theta_t, 0, \eta_t)$ and apply the triangle inequality:

$$d_F(\theta_{t+1}, \theta_t) \leq d_F(\theta_{t+1}, F(\theta_t, 0, \eta_t)) + d_F(F(\theta_t, 0, \eta_t), \theta_t).$$

By definition of the exogenous drift magnitude (Section 3),

$$d_t := d_F(F(\theta_t, 0, \eta_t), \theta_t),$$

so it remains to control the first term.

Control the policy-sensitive displacement. By the local comparison assumption on K (Equation (12)), there exists $\alpha > 0$ such that

$$d_F(\theta_{t+1}, F(\theta_t, 0, \eta_t)) \leq \alpha \kappa_t^{(\mathcal{M})} + \epsilon_t,$$

where $\kappa_t^{(\mathcal{M})}$ is defined in (8) and $\epsilon_t := \|r_t\|_{g_{F(\theta_t, 0, \eta_t)}}$ satisfies the quadratic bound $\epsilon_t \leq c\|u_t\|^2$ by (10).

Combining the previous two results gives the one-step motion bound

$$d_F(\theta_{t+1}, \theta_t) \leq d_t + \alpha \kappa_t^{(\mathcal{M})} + \epsilon_t.$$

Sum over time. Summing over $t = 1, \dots, T$ yields

$$\mathcal{A}_T = \sum_{t=1}^T d_F(\theta_{t+1}, \theta_t) \leq \sum_{t=1}^T (d_t + \alpha \kappa_t^{(\mathcal{M})} + \epsilon_t) = C_T + \sum_{t=1}^T \epsilon_t,$$

where $C_T := \sum_{t=1}^T (d_t + \alpha \kappa_t^{(\mathcal{M})})$ is the intrinsic drift budget. The remainder bound $\epsilon_t \leq c\|u_t\|^2$ follows from (10). \square

A.4 Proof of Lemma 6 (Summed drift penalty)

Proof. Recall

$$V_T(f, \pi) := \frac{1}{T} \sum_{t=1}^T |R(\theta_{t+1}, f_t) - R(\theta_t, f_t)|.$$

Fix any learner (f, π) generating the trajectory $\{(\theta_t, u_t)\}_{t=1}^T$.

One-step risk motion bound. For each t , Assumption 3 applied with $\theta = \theta_t$ and $\theta' = \theta_{t+1}$ (and predictor f_t fixed) yields the pathwise inequality

$$|R(\theta_{t+1}, f_t) - R(\theta_t, f_t)| \leq L_p d_F(\theta_{t+1}, \theta_t). \quad (26)$$

Summing (26) over $t = 1, \dots, T$ and dividing by T gives

$$V_T(f, \pi) \leq \frac{L_p}{T} \sum_{t=1}^T d_F(\theta_{t+1}, \theta_t) = \frac{L_p}{T} \mathcal{A}_T, \quad (27)$$

where $\mathcal{A}_T := \sum_{t=1}^T d_F(\theta_{t+1}, \theta_t)$ is the cumulative Fisher–Rao path length.

Invoke the information path bound. By Equation 15, the path length satisfies the pathwise bound

$$\mathcal{A}_T \leq C_T + \sum_{t=1}^T \epsilon_t, \quad \epsilon_t \leq c \|u_t\|^2.$$

Substituting into (27) yields

$$V_T(f, \pi) \leq \frac{L_p}{T} \left(C_T + \sum_{t=1}^T \epsilon_t \right) \leq \frac{L_p}{T} C_T + \frac{L_p c}{T} \sum_{t=1}^T \|u_t\|^2,$$

which proves the first two results.

Take expectations. Taking expectations of the previous inequality and using linearity of expectation gives

$$\mathbb{E} V_T(f, \pi) \leq \frac{L_p}{T} \mathbb{E}[C_T] + \frac{L_p c}{T} \sum_{t=1}^T \mathbb{E} \|u_t\|^2,$$

which is the final result. \square

A.5 Proof of Theorem 1 (Prequential reproducibility bound)

Proof. By the add–subtract decomposition (7), we have the pathwise bound

$$\Delta_T^{\text{rep}}(f, \pi) \leq \Delta_T^{\text{sam}}(f, \pi) + V_T(f, \pi).$$

Taking expectations gives

$$\mathbb{E} \Delta_T^{\text{rep}}(f, \pi) \leq \mathbb{E} \Delta_T^{\text{sam}}(f, \pi) + \mathbb{E} V_T(f, \pi). \quad (28)$$

Sampling term. Recall $\Delta_T^{\text{sam}}(f, \pi) = \left| \frac{1}{T} \sum_{t=1}^T Z_t \right|$ with $Z_t := \ell(f_t(x_t), y_t) - R(\theta_t, f_t)$ (Section 3). Under the endogenous–drift model (6), $(Z_t)_{t=1}^T$ is a martingale difference sequence with respect to the filtration $\{\mathcal{F}_t\}$, and Assumption 1(4) gives the conditional σ –sub-Gaussian mgf bound required by Lemma 3. Therefore Corollary 1 yields

$$\mathbb{E} \Delta_T^{\text{sam}}(f, \pi) = \mathbb{E} \left| \frac{1}{T} \sum_{t=1}^T Z_t \right| \leq \frac{\sqrt{2\pi} \sigma}{\sqrt{T}}. \quad (29)$$

Drift term. By Lemma 6 (proved in Appendix A.4),

$$V_T(f, \pi) \leq \frac{L_p}{T} C_T + \frac{L_p c}{T} \sum_{t=1}^T \|u_t\|^2.$$

Taking expectations gives

$$\mathbb{E} V_T(f, \pi) \leq \frac{L_p}{T} \mathbb{E}[C_T] + \frac{L_p c}{T} \sum_{t=1}^T \mathbb{E} \|u_t\|^2. \quad (30)$$

Combine. Substituting (29) and (30) into (28) yields the stated bound. \square

A.6 Proof of Theorem 2 (Lower Bound)

Proof. We follow standard minimax lower-bound arguments based on two-point and multiple-hypothesis testing reductions; see Tsybakov and Zaiats (2009, Ch. 2).

We construct an explicit subclass \mathcal{P}_C of drift–feedback processes satisfying Assumptions 1–2 and $\mathbb{E}_P[C_T] \leq C$ on which estimating

$$R_T^+(P) := \frac{1}{T} \sum_{t=1}^T R(\theta_{t+1}, f_t), \quad \mathcal{L}_t(\theta) := R(\theta, f_t),$$

so that $R_T^+(P) = \frac{1}{T} \sum_{t=1}^T \mathcal{L}_t(\theta_{t+1})$ incurs minimax error $\gtrsim \max(T^{-1/2}, C/T)$.

Local model and Fisher geometry. Work in a one-dimensional regular exponential family $\{p_\theta\}$ on the observation space (equivalently, take \mathcal{Y} trivial and write $(x_t, y_t) \equiv x_t$):

$$p_\theta(x) = \exp(\theta x - A(\theta)) h(x), \quad \theta \in \Theta \subset \mathbb{R},$$

restricted to a compact interval on which the Fisher information $I(\theta) = A''(\theta)$ is bounded above and below. This satisfies Assumption 1. Introduce the Fisher arclength coordinate

$$s(\theta) := \int_{\theta_0}^{\theta} \sqrt{I(u)} du,$$

and restrict to a neighborhood of θ_0 where s is a diffeomorphism. In the s -coordinate the Fisher metric is identically 1, hence locally

$$d_F(\theta, \theta') = |s(\theta) - s(\theta')|.$$

For convenience we work in arclength coordinates and write this coordinate again as θ , so that $d_F(\theta, \theta') = |\theta - \theta'|$ on the neighborhood under consideration.

Deterministic controlled dynamics and budget. Consider deterministic controlled dynamics

$$\theta_{t+1} = F(\theta_t, u_t, \eta_t) = \theta_t + u_t, \quad \eta_t \equiv 0.$$

Then $d_t \equiv 0$, $J_u F \equiv 1$, and the Taylor remainder vanishes. In arclength coordinates ($g \equiv 1$) we have $\kappa_t^{(\mathcal{M})} = |u_t|$, and therefore

$$C_T = \alpha \sum_{t=1}^T |u_t|.$$

Block construction and codebook. Fix a step size $\delta > 0$ and let $m \leq \lfloor T/2 \rfloor$. Partition the horizon into m disjoint two-step blocks $B_j = \{2j-1, 2j\}$, $j = 1, \dots, m$, and set $u_t \equiv 0$ for $t > 2m$.

Let $V \subset \{-1, +1\}^m$ be a binary code with minimum Hamming distance at least βm and cardinality $|V| \geq 2^{\zeta m}$ for constants $\beta, \zeta > 0$ (Tsybakov and Zaiats, 2009, Lemma 2.9). For each $v = (v_1, \dots, v_m) \in V$ define deterministic controls

$$u_{2j-1}^{(v)} = v_j \delta, \quad u_{2j}^{(v)} = -v_j \delta, \quad u_t^{(v)} = 0 \quad (t > 2m).$$

Starting from $\theta_1 = \theta_0$, the resulting trajectory satisfies

$$\theta_{2j-1}^{(v)} = \theta_0, \quad \theta_{2j}^{(v)} = \theta_0 + v_j \delta, \quad \theta_{2j+1}^{(v)} = \theta_0,$$

and $\theta_t^{(v)} = \theta_0$ for $t > 2m$. Each block performs a geodesic excursion out-and-back of length 2δ , so

$$C_T(P_v) = \alpha \sum_{t=1}^T |u_t^{(v)}| = 2\alpha m \delta.$$

Choose

$$m := \left\lfloor \frac{C}{2\alpha\delta} \right\rfloor \wedge \left\lfloor \frac{T}{2} \right\rfloor \quad \text{so that} \quad C_T(P_v) \leq C \quad \text{for all } v \in V. \quad (31)$$

(In this subclass C_T is deterministic, hence $\mathbb{E}_{P_v}[C_T] \leq C$.)

Separation in the one-step-ahead risk functional. Fix a learner sequence $(f_t)_{t=1}^T$ and loss/model pair such that the population risk has a nonzero local slope at θ_0 on the indices $t = 2j - 1$ used below: there exists $c_0 > 0$ such that $|\partial_\theta \mathcal{L}_{2j-1}(\theta_0)| \geq c_0$ for all $j \leq m$. Then for sufficiently small δ ,

$$\mathcal{L}_{2j-1}(\theta_0 + \delta) - \mathcal{L}_{2j-1}(\theta_0 - \delta) = 2\delta \partial_\theta \mathcal{L}_{2j-1}(\theta_0) + O(\delta^2),$$

so there exists $c_\ell > 0$ such that whenever $v_j \neq w_j$,

$$|\mathcal{L}_{2j-1}(\theta_{2j}^{(v)}) - \mathcal{L}_{2j-1}(\theta_{2j}^{(w)})| = |\mathcal{L}_{2j-1}(\theta_0 + v_j \delta) - \mathcal{L}_{2j-1}(\theta_0 + w_j \delta)| \geq c_\ell \delta.$$

Because v and w differ in at least βm blocks, and because $R_T^+(P_v) = \frac{1}{T} \sum_{t=1}^T \mathcal{L}_t(\theta_{t+1}^{(v)})$ depends on the excursions exactly at the indices $t = 2j - 1$ via $\theta_{t+1}^{(v)} = \theta_{2j}^{(v)}$, we obtain the packing separation

$$|R_T^+(P_v) - R_T^+(P_w)| \geq \frac{1}{T} \sum_{j: v_j \neq w_j} |\mathcal{L}_{2j-1}(\theta_{2j}^{(v)}) - \mathcal{L}_{2j-1}(\theta_{2j}^{(w)})| \geq \frac{\beta m c_\ell \delta}{T}. \quad (32)$$

With the choice (31), this lower bound is of order $(m\delta)/T \asymp C/T$.

KL divergence control. For each v , the state path $\{\theta_t^{(v)}\}$ is deterministic. Conditional on $\theta_t^{(v)}$, the observation at time t is drawn from $p_{\theta_t^{(v)}}$, so the joint law factorizes and

$$D_{\text{KL}}(P_v \| P_w) = \sum_{t=1}^T D_{\text{KL}}(p_{\theta_t^{(v)}} \| p_{\theta_t^{(w)}}).$$

The trajectories differ only at times $t = 2j$ where $v_j \neq w_j$. On a compact neighborhood, regular exponential families satisfy a uniform quadratic KL bound: there exists $C_I < \infty$ such that for sufficiently small δ ,

$$D_{\text{KL}}(p_{\theta_0+\delta} \| p_{\theta_0-\delta}) \leq C_I \delta^2.$$

Hence

$$D_{\text{KL}}(P_v \| P_w) \leq C_I m \delta^2. \quad (33)$$

Fano lower bound for the C/T term. Choose δ small enough (depending only on fixed model constants) so that the Fano condition holds, e.g. $C_I m \delta^2 \leq \frac{1}{8} \log |V|$, using (33) and $\log |V| \geq \zeta m$. Applying the multi-hypothesis Fano inequality to the packing $\{P_v\}_{v \in V} \subset \mathcal{P}_C$ and the separation (32) yields

$$\inf_{\widehat{R}_T} \sup_{P \in \mathcal{P}_C} \mathbb{E}_P |\widehat{R}_T - R_T^+(P)| \gtrsim \frac{m\delta}{T} \asymp \frac{C}{T}.$$

The $T^{-1/2}$ term from a stationary subclass. To obtain the classical term, restrict further to a stationary subclass ($C_T \equiv 0$) where $\theta_t \equiv \theta$ is fixed over time. Then $R_T^+(P) = \frac{1}{T} \sum_{t=1}^T \mathcal{L}_t(\theta)$ is a one-dimensional smooth functional of θ . A standard two-point Le Cam argument over $\theta \in \{\theta_0 \pm \delta/\sqrt{T}\}$ (using the same local quadratic KL control) gives

$$\inf_{\widehat{R}_T} \sup_{P: C_T \equiv 0} \mathbb{E}_P |\widehat{R}_T - R_T^+(P)| \gtrsim T^{-1/2}.$$

Combine regimes. Since the stationary subclass is contained in \mathcal{P}_C for any $C \geq 0$, combining the two lower bounds yields

$$\inf_{\widehat{R}_T} \sup_{P \in \mathcal{P}_C} \mathbb{E}_P |\widehat{R}_T - R_T^+(P)| \gtrsim \max\left(T^{-1/2}, \frac{C}{T}\right),$$

which proves the theorem (absorbing constants into c_1). \square

A.7 Proofs of Limiting Regimes (Stationary and Classical Limits)

Lemma 8 (Stationary (i.i.d.) regime). *If $d_t \equiv 0$ and $J_u F \equiv 0$ for all t , then $\theta_t = \theta_0$ for all t , so $p_{\theta_t} = p_{\theta_0}$ and the samples are drawn from a stationary law. Moreover $V_T(f, \pi) = 0$ and*

$$\mathbb{E} \Delta_T^{\text{rep}}(f, \pi) \leq \mathbb{E} \Delta_T^{\text{sam}}(f, \pi) \leq \frac{\sqrt{2\pi} \mathcal{V}_T}{T} \leq \frac{\sqrt{2\pi} \sigma}{\sqrt{T}},$$

under the standing σ -sub-Gaussian increment condition.

Proof. If $d_t \equiv 0$ and $J_u F \equiv 0$, then the update does not move the environment, hence $\theta_{t+1} = \theta_t$ and $\theta_t = \theta_0$ for all t . Therefore $R(\theta_{t+1}, f_t) = R(\theta_t, f_t)$ for every t and $V_T(f, \pi) = 0$. The decomposition in the main text gives $\Delta_T^{\text{rep}}(f, \pi) \leq \Delta_T^{\text{sam}}(f, \pi) + V_T(f, \pi) = \Delta_T^{\text{sam}}(f, \pi)$. The sampling term is an average of martingale differences, so the stated bound follows from Corollary 1. \square

Lemma 9 (Exogenous-drift regime). *If $J_u F \equiv 0$ (no policy-induced motion), then the drift penalty is controlled purely by the exogenous budget and*

$$V_T(f, \pi) \leq \frac{L_p}{T} C_T \quad \text{and} \quad \mathbb{E} \Delta_T^{\text{rep}}(f, \pi) \leq \mathbb{E} \Delta_T^{\text{sam}}(f, \pi) + \frac{L_p}{T} \mathbb{E}[C_T].$$

In particular, when $C_T = \sum_{t=1}^T d_t$ in this regime, this matches the classical “variation budget” penalty scaling $\sum_t d_t/T$.

Proof. With $J_u F \equiv 0$, the endogenous component vanishes and the controls do not contribute to motion. Equation 6 gives $V_T(f, \pi) \leq \frac{L_p}{T} (C_T + \sum_t \epsilon_t)$. Combine with $\Delta_T^{\text{rep}} \leq \Delta_T^{\text{sam}} + V_T$ and take expectations. \square

Lemma 10 (Adaptive-data / purely endogenous regime). *If $d_t \equiv 0$ (no exogenous drift), then all motion is policy-induced and*

$$V_T(f, \pi) \leq \frac{L_p}{T} C_T + \frac{L_p c}{T} \sum_{t=1}^T \|u_t\|^2,$$

hence

$$\mathbb{E} \Delta_T^{\text{rep}}(f, \pi) \leq \mathbb{E} \Delta_T^{\text{sam}}(f, \pi) + \frac{L_p}{T} \mathbb{E}[C_T] + \frac{L_p c}{T} \sum_{t=1}^T \mathbb{E}\|u_t\|^2.$$

Proof. This is immediate from Equation 6 after setting $d_t \equiv 0$, and then combining with $\Delta_T^{\text{rep}} \leq \Delta_T^{\text{sam}} + V_T$ followed by expectations. \square

Synthesis. In all regimes,

$$\mathbb{E} \Delta_T^{\text{rep}}(f, \pi) \leq \mathbb{E} \Delta_T^{\text{sam}}(f, \pi) + \mathbb{E} V_T(f, \pi) = O\left(T^{-1/2} + \frac{\mathbb{E}[C_T]}{T}\right) \quad (\text{up to the control-energy remainder}).$$

Thus $T^{-1/2}$ recovers the classical sampling rate when the environment is stationary, while $\mathbb{E}[C_T]/T$ quantifies the additional irreducible penalty due to distributional motion.

B Experimental Details

This appendix specifies the simulators, metrics, parameter grids, and evaluation protocols used to produce all figures in Section 7. All experiments were implemented in Python 3.11 using NumPy, SciPy, and PyTorch (for the nonlinear learner). Per-run integer seeds ensure deterministic reproduction of all reported results.

Recorded quantities and paper-aligned timing. Across all settings we record the environment trajectory $\{\theta_t\}$, the learner trajectory $\{f_t\}$, the empirical trajectory loss

$$\hat{R}_T = \frac{1}{T} \sum_{t=1}^T \ell(f_t(x_t), y_t),$$

and an approximation of the corresponding population loss $R_T = \frac{1}{T} \sum_{t=1}^T R(\theta_t, f_t)$, computed either in closed form (linear–Gaussian environment) or using clean mini-batches drawn from the latent generative model (nonlinear environment). We report the trajectory generalization gap $|\hat{R}_T - R_T|$ and (when drift is present) the prequential gap

$$\Delta_T^{\text{rep}} = |\hat{R}_T - R_T^+|, \quad R_T^+ = \frac{1}{T} \sum_{t=1}^T R(\theta_{t+1}, f_t).$$

In all simulators, predictors f_t (and any controls u_t) are constructed to be \mathcal{F}_{t-1} -measurable (“predict then observe”), matching the measurability convention used in the theoretical decomposition $\Delta_T^{\text{rep}} \leq \Delta_T^{\text{sam}} + V_T$.

Closed-loop drift telemetry. When the drift decomposition is available (linear–Gaussian) or approximated (nonlinear teacher–learner), we log the per-step Fisher-metric magnitudes

$$d_t = \|\Delta\theta_t^{\text{exo}}\|_{g_{\theta_t}}, \quad \kappa_t^{(\mathcal{M})} = \|\Delta\theta_t^{\text{endo}}\|_{g_{\theta_t}}, \quad \bar{d} = \frac{1}{T} \sum_{t=1}^T d_t, \quad \bar{\kappa} = \frac{1}{T} \sum_{t=1}^T \kappa_t^{(\mathcal{M})}.$$

We also log the drift penalty

$$V_T = \frac{1}{T} \sum_{t=1}^T |R(\theta_{t+1}, f_t) - R(\theta_t, f_t)|,$$

which isolates environment motion by holding f_t fixed within each step.

B.1 Linear–Gaussian demonstration: budget collapse and horizon scaling

We use a closed-form Gaussian mean estimation model to instantiate the quantities in Section 7.1. The environment state is $\theta_t \in \mathbb{R}^d$ and observations are

$$x_t \sim \mathcal{N}(\theta_t, \Sigma), \quad \ell(f, x) = \|x - f\|_2^2.$$

The deployed predictor is the paper-aligned online mean $f_t = \hat{\mu}_{t-1}$, where $\hat{\mu}_t = \frac{1}{t} \sum_{i=1}^t x_i$. Population risk is available in closed form:

$$R(\theta, \mu) = \mathbb{E}\|X - \mu\|_2^2 = \text{tr}(\Sigma) + \|\theta - \mu\|_2^2.$$

Accordingly we compute $R_T = \frac{1}{T} \sum_t R(\theta_t, f_t)$ exactly and evaluate \hat{R}_T from realized losses.

(a) Budgeted scaling of the drift component V_T . To isolate the drift contribution, we evaluate the drift term

$$V_T = \frac{1}{T} \sum_{t=1}^T |R(\theta_{t+1}, f_t) - R(\theta_t, f_t)|$$

under Fisher-budgeted exogenous motion and \mathcal{F}_{t-1} -measurable feedback. We use $d = 5$, $\Sigma = I_d$ (so $g_{\theta} = \Sigma^{-1}$ is constant), $T = 2000$, and 12 seeds. For each run we construct an exogenous increment v_t^{exo} by drawing a random direction and rescaling it to have Fisher length C_{exo}/T , and we set the endogenous action to be history-measurable via $u_t = -k \hat{\mu}_{t-1}$ with fixed $k = 0.25$ and feedback strength γ . We sweep

$$C_{\text{exo}} \in \{0, 2, 4, 8, 16, 32\}, \quad \gamma \in \{0, 0.01, 0.02, 0.04, 0.08\},$$

which induces four regimes (iid, exogenous-only, endogenous-only, mixed). We record the Fisher magnitudes

$$\bar{d} = \frac{1}{T} \sum_{t=1}^T \|v_t^{\text{exo}}\|_{\Sigma^{-1}}, \quad \bar{\kappa} = \frac{1}{T} \sum_{t=1}^T \|\gamma u_t\|_{\Sigma^{-1}},$$

and fit α_* by linear regression so that the combined budget predictor $C_T/T = \bar{d} + \alpha_* \bar{\kappa}$ collapses V_T across regimes (Figure 3(a)).

(b) Horizon scaling of sampling versus drift. To illustrate how the decomposition separates horizon effects, we fix a persistent bounded drift level and sweep the horizon T . We use a

reflecting-walk construction to keep θ_t in a compact set while enforcing approximately constant per-step Fisher motion δ_F (with $\Sigma = \sigma^2 I_d$ so the Euclidean step is $\delta_F \sigma$). We evaluate $T \in \{200, 400, 800, 1600, 3200, 6400, 12800\}$ with 40 seeds and drift levels $\delta_F \in \{0, 0.1, 0.2\}$ (including the iid baseline). At $\delta_F = 0.1$ we plot $\Delta_T^{\text{sam}} = |\hat{R}_T - R_T|$ together with V_T as functions of T , with iid reference: Δ_T^{sam} decreases with T , while V_T remains approximately stable, so the dominant contribution transitions from sampling-driven to drift-driven at large horizons (Figure 3(b)).

B.2 Nonlinear Speed–Limit Validation (teacher–learner)

Objective. To test whether the empirical organization $\Delta_T^{\text{rep}} \approx b_0 + b_s T^{-1/2} + b_1 \bar{d} + b_2 \bar{\kappa}$ and the reduced dependence on C_T/T persist in a nonlinear closed-loop setting.

Latent teacher model. Inputs are i.i.d. Gaussian $x_t \sim \mathcal{N}(0, I_d)$ with $d = 5$. A fixed random feature map $\phi : \mathbb{R}^d \rightarrow \mathbb{R}^m$ with $m = 64$ is constructed as

$$\phi(x) = \tanh(Wx + b),$$

with $W_{ij} \sim \mathcal{N}(0, 1/d)$ and $b_i \sim \mathcal{N}(0, 0.1^2)$ (seeded once). The environment state is $\theta_t \in \mathbb{R}^m$ and labels are generated by

$$y_t = \phi(x_t)^\top \theta_t + \sigma \xi_t, \quad \xi_t \sim \mathcal{N}(0, 1),$$

with $\sigma = 0.1$.

Learner. The learner is a two-layer MLP $f_t : \mathbb{R}^d \rightarrow \mathbb{R}$ with hidden width 128 and tanh nonlinearity, trained online using single-sample SGD (learning rate 0.1). Gradients are clipped to max norm 1.0. Training loss is the noisy squared loss $\ell(f(x), y) = (f(x) - y)^2$.

Fisher metric proxy in teacher space. We define a Fisher–Gram matrix in θ -space using probe covariates X_p :

$$G(\theta) \approx \frac{1}{N\sigma^2} \Phi(X_p)^\top \Phi(X_p) \quad \text{where} \quad \Phi(X_p) = [\phi(x)]_{x \in X_p}.$$

In our implementation we use a fixed probe batch of size $N = 512$ and add a small ridge ($10^{-6}I$) for numerical stability. The Fisher norm proxy is $\|v\|_G = \sqrt{v^\top G v}$.

Exogenous drift budget manager. At each step we draw a random direction $r_t \sim \mathcal{N}(0, I_m)$ in θ -space and a proposed Fisher length ℓ_t^{exo} from an exponential distribution with mean C_{exo}/T . A budget manager clips the applied step to the remaining exogenous budget, producing $\Delta\theta_t^{\text{exo}}$ with logged length $d_t = \|\Delta\theta_t^{\text{exo}}\|_G$ and $\sum_t d_t \leq C_{\text{exo}}$.

Policy-sensitive drift direction. We derive a policy-sensitive direction from teacher–student disagreement on a fresh probe batch X_{probe} of size 256. Let $g_\theta(x) = \phi(x)^\top \theta$ be the teacher mean and compute residuals $r(x) = f_t(x) - g_\theta(x)$. The direction is a (normalized) gradient in θ -space:

$$\nabla_\theta = -\frac{2}{|X_{\text{probe}}|} \sum_{x \in X_{\text{probe}}} \phi(x) r(x).$$

We normalize and clip this direction in Fisher norm to prevent rare probe batches from producing extreme steps. An endogenous budget manager then takes a step of target Fisher length ℓ_t^{endo} (constant mean per step) clipped to remaining endogenous budget. We log $\kappa_t^{(\mathcal{M})} = \|\Delta\theta_t^{\text{endo}}\|_G$.

Endogenous budget scaling and γ . We parameterize feedback strength by a scalar γ that scales the *total* endogenous budget linearly with T , so that the *average per-step* endogenous Fisher length is proportional to γ . Concretely, we use a fixed constant $C_{\text{pol}} = 8$ and policy coefficient $k = 0.25$ and set the total endogenous budget to

$$C_{\text{endo}}(T, \gamma) = \gamma \cdot k \cdot C_{\text{pol}} \cdot T,$$

so the mean endogenous length per step is

$$\frac{C_{\text{endo}}}{T} = \gamma k C_{\text{pol}}.$$

(When $\gamma = 0$, the endogenous channel is disabled.)

Evaluation protocol (critical for nonstationary trajectories). Population MSE is approximated by Monte Carlo on *fresh* covariates:

$$R(\theta, f) = \mathbb{E}[(f(x) - y)^2] = \mathbb{E}[(f(x) - \phi(x)^\top \theta)^2] + \sigma^2,$$

estimated using batches of size $N_{\text{pop}} = 2048$. Because the process is nonstationary, \hat{R}_T and R_T^+ must be computed on a *common schedule*. We therefore evaluate every `eval_every=10` steps and always at $t = T$, and we *subsample* the empirical training loss on exactly the same evaluation times. On evaluation steps we compute the paired risks $R(\theta_t, f_t)$ and $R(\theta_{t+1}, f_t)$ on the *same* batch of covariates, then record $|R(\theta_{t+1}, f_t) - R(\theta_t, f_t)|$ for V_T .

Grids and held-out horizon. We sweep horizons $T \in \{800, 1600, 3200, 6400\}$, exogenous ratios $C_{\text{exo}}/T \in \{2.5, 5, 10, 20, 40, 80\} \times 10^{-3}$ (so $C_{\text{exo}} = (C_{\text{exo}}/T) \cdot T$), and feedback strengths $\gamma \in \{0, 0.0025, 0.005, 0.01, 0.02\}$, using 12 seeds. We fit the additivity plane on all horizons except a held-out $T_{\text{hold}} = 6400$, set $\alpha_\star = b_2/b_1$, then evaluate the reduced C_T/T model on the held-out horizon.

Reported diagnostics. In addition to Δ_T^{rep} , we log (i) V_T , (ii) $\sum_t d_t$ and $\sum_t \kappa_t^{(\mathcal{M})}$, (iii) observed-versus-predicted scatter for the fitted plane, and (iv) initial versus final population MSE to confirm that the learner is improving and that observed effects are due to drift rather than optimization instability.

B.3 Observable Fisher motion under monitoring channels

Objective. To validate the monotonicity bridge of Section 6 in a setting where both intrinsic Fisher–Rao step lengths and their channel-induced counterparts are available in closed form. The experiment tests two claims: (i) *stepwise contraction* of Fisher–Rao distance under a fixed Markov kernel K , and (ii) *rate tracking* of regime changes via trailing-window averages of Fisher step lengths after the channel.

Intrinsic environment model. We use the Gaussian location family

$$P_t = \mathcal{N}(\theta_t, \Sigma), \quad \Sigma \in \mathbb{R}^{d \times d} \text{ fixed,}$$

with $d = 5$ and $\Sigma = I_d$. The environment state evolves according to a mixed exogenous/endogenous drift–feedback update,

$$\theta_{t+1} = \theta_t + v_t^{\text{exo}} + \gamma u_t, \quad u_t = -k \hat{\mu}_{t-1},$$

where $\hat{\mu}_{t-1}$ is the online mean estimator computed from past samples (measurable with respect to \mathcal{F}_{t-1}), $k > 0$ is a fixed feedback gain, and $\gamma \geq 0$ controls feedback strength. Exogenous increments are generated by drawing random directions and rescaling them to have a prescribed per-step Fisher length, so that the cumulative exogenous motion is budgeted over the horizon. The implementation follows the same Gaussian drift pipeline used in the main linear validation.

Intrinsic Fisher motion (closed form). In the Gaussian location family, Fisher–Rao step length reduces to a Mahalanobis norm:

$$d_F(P_{t+1}, P_t) = \|\theta_{t+1} - \theta_t\|_{\Sigma^{-1}}, \quad A_T(P) = \sum_{t=1}^T d_F(P_{t+1}, P_t).$$

We record the intrinsic one-step lengths $\ell_t(P) := d_F(P_{t+1}, P_t)$ for $t = 1, \dots, T$.

Monitoring channel and induced motion. We model partial observability via a fixed linear Gaussian Markov kernel K acting on each sample x :

$$o = Bx + \xi, \quad \xi \sim \mathcal{N}(0, \sigma_K^2 I_k),$$

where $B \in \mathbb{R}^{k \times d}$ is a fixed random projection with row normalization. The induced output law remains Gaussian,

$$Q_t := K_{\#} P_t = \mathcal{N}(B\theta_t, S), \quad S := B\Sigma B^\top + \sigma_K^2 I_k,$$

so Fisher–Rao step lengths are again closed form:

$$d_F(Q_{t+1}, Q_t) = \|B(\theta_{t+1} - \theta_t)\|_{S^{-1}}, \quad A_T^{(K)} = \sum_{t=1}^T d_F(Q_{t+1}, Q_t).$$

We evaluate three channels in a single run to illustrate varying degrees of contraction: a baseline (k, σ_K) pair, a less lossy channel (larger k and smaller σ_K), and a more lossy channel (smaller k and larger σ_K).

Rate visualization via burst scheduling. To highlight the rate interpretation, we allocate the *same* total exogenous budget across time using bursty weights. Specifically, the per-step exogenous Fisher length is scaled by a piecewise-constant weight sequence with mean 1, with contiguous “high” segments of multiplicative factor `burst_hi` occurring once per period `burst_period` (with a random phase within each period), and “low” segments chosen to preserve mean 1. This produces alternating low- and high-speed intervals while keeping the total exogenous budget fixed. We report local drift

speed via a trailing-window average of step lengths:

$$\bar{a}_t(P) := \frac{1}{|W_t|} \sum_{s \in W_t} d_F(P_{s+1}, P_s), \quad \bar{a}_t(K_{\#}P) := \frac{1}{|W_t|} \sum_{s \in W_t} d_F(Q_{s+1}, Q_s),$$

where W_t is the trailing window of length `rate_window` (shortened near the start of the trajectory). The left panel of Figure 6 plots $\bar{a}_t(P)$ and $\bar{a}_t(K_{\#}P)$ to show that observed rates follow the same burst structure while remaining uniformly smaller.

Contraction check. We verify stepwise contraction by plotting the scatter of $\ell_t(P) = d_F(P_{t+1}, P_t)$ versus $\ell_t(Q) = d_F(Q_{t+1}, Q_t)$ across t for each channel, together with the diagonal $y = x$. The right panel of Figure 6 corresponds to this check.

References

- Shun-ichi Amari. *Information Geometry and Its Applications*. Springer, Tokyo, 2016. doi: 10.1007/978-4-431-55978-8.
- Shun-ichi Amari, Ryo Karakida, and Masafumi Oizumi. Fisher information and natural gradient learning in random deep networks. In Kamalika Chaudhuri and Masashi Sugiyama, editors, *Proceedings of the Twenty-Second International Conference on Artificial Intelligence and Statistics*, volume 89 of *Proceedings of Machine Learning Research*, pages 694–702, Naha, Okinawa, Japan, 16–18 Apr 2019. PMLR.
- Shun-ichi Amari and Hiroshi Nagaoka. *Methods of Information Geometry*, volume 191 of *Translations of Mathematical Monographs*. American Mathematical Society & Oxford University Press, Providence, Rhode Island, 2000. ISBN 978-0-8218-4302-4.
- Raef Bassily, Kobbi Nissim, Adam Smith, Thomas Steinke, Uri Stemmer, and Jonathan Ullman. Algorithmic stability for adaptive data analysis? In Yishay Mansour and Daniel Wichs, editors, *Proceedings of the 48th Annual ACM SIGACT Symposium on Theory of Computing (STOC 2016)*, pages 1046–1059, Cambridge, MA, USA, 2016. Association for Computing Machinery. doi: 10.1145/2897518.2897566.
- Omar Besbes, Yonatan Gur, and Assaf Zeevi. Non-stationary stochastic optimization. *Operations Research*, 63(5):1227–1244, 2015. doi: 10.1287/opre.2015.1408.
- Gilles Blanchard, Aniket Anand Deshmukh, Urun Doğan, Gyemin Lee, and Clayton Scott. Domain generalization by marginal transfer learning. *Journal of Machine Learning Research*, 22(17-679): 1–55, 2021.
- Cynthia Dwork, Vitaly Feldman, Moritz Hardt, Toniann Pitassi, Omer Reingold, and Aaron Roth. Generalization in adaptive data analysis and holdout reuse. In *Advances in Neural Information Processing Systems*, volume 28, 2015.
- Eyal Even-Dar and Yishay Mansour. Learning rates for q-learning. *Journal of Machine Learning Research*, 5(Dec):1–25, 2003.
- Pascal Germain, Amaury Habrard, François Laviolette, and Emilie Morvant. A PAC-bayesian theory for domain adaptation. In *Proceedings of the 33rd International Conference on Machine*

- Learning*, volume 48 of *Proceedings of Machine Learning Research*, pages 820–829, New York, New York, 2016. PMLR.
- Sebastian Goldt and Udo Seifert. Stochastic thermodynamics of learning. *Physical Review Letters*, 118(1):010601, 2017. doi: 10.1103/PhysRevLett.118.010601.
- Eric Hall and Rebecca Willett. Dynamical models and tracking regret in online convex programming. In Sanjoy Dasgupta and David McAllester, editors, *Proceedings of the 30th International Conference on Machine Learning*, volume 28 of *Proceedings of Machine Learning Research*, pages 579–587, Atlanta, Georgia, USA, 17–19 Jun 2013. PMLR.
- Zachary Izzo, Lexing Ying, and James Zou. How to learn when data reacts to your model: Performative gradient descent. In Marina Meila and Tong Zhang, editors, *Proceedings of the 38th International Conference on Machine Learning*, volume 139 of *Proceedings of Machine Learning Research*, pages 4641–4650, Online, 2021. PMLR.
- Meena Jagadeesan, Tijana Zrnic, and Celestine Mendler-Dünner. Regret minimization with performative feedback. In Kamalika Chaudhuri, Stefanie Jegelka, Le Song, Csaba Szepesvari, Gang Niu, and Sivan Sabato, editors, *Proceedings of the 39th International Conference on Machine Learning*, volume 162 of *Proceedings of Machine Learning Research*, pages 9760–9785, Baltimore, Maryland, Jul 17–23 2022. PMLR.
- Vitaly Kuznetsov and Mehryar Mohri. Time series prediction and online learning. In Vitaly Feldman, Alexander Rakhlin, and Ohad Shamir, editors, *29th Annual Conference on Learning Theory*, volume 49 of *Proceedings of Machine Learning Research*, pages 1190–1213, Columbia University, New York, NY, USA, 23–26 Jun 2016. PMLR.
- John M. Lee. *Riemannian Manifolds: An Introduction to Curvature*, volume 176 of *Graduate Texts in Mathematics*. Springer, New York, 1997. doi: 10.1007/b98852.
- Jiachun Li, David Simchi-Levi, and Yunxiao Zhao. Optimal adaptive experimental design for estimating treatment effect, 2024.
- Mehryar Mohri and Andres Muñoz Medina. New analysis and algorithm for learning with drifting distributions. ALT’12, page 124–138, Berlin, Heidelberg, 2012. Springer-Verlag. ISBN 9783642341052. doi: 10.1007/978-3-642-34106-9_13.
- Noboru Murata, Motoaki Kawanabe, Andreas Ziehe, Klaus-Robert Müller, and Shun ichi Amari. Online learning in changing environments with applications in supervised and unsupervised learning. *Neural Networks*, 15(4):743–760, 2002. ISSN 0893-6080. doi: 10.1016/S0893-6080(02)00060-6.
- Pedro A. Ortega and Daniel A. Braun. Thermodynamics as a theory of decision-making with information-processing costs. *Proceedings of the Royal Society A: Mathematical, Physical and Engineering Sciences*, 469(2153), 2013. doi: 10.1098/rspa.2012.0683.
- Juan C. Perdomo, Tijana Zrnic, Celestine Mendler-Dünner, and Moritz Hardt. Performative prediction. In *Proceedings of the 37th International Conference on Machine Learning (ICML)*, pages 7599–7609, Online, 2020. PMLR.
- C. R. Rao. Information and the accuracy attainable in the estimation of statistical parameters. *Bulletin of the Calcutta Mathematical Society*, 37:81–91, 1945.

- Ryan Rogers, Aaron Roth, Adam Smith, Nathan Srebro, Om Thakkar, and Blake Woodworth. Guaranteed validity for empirical approaches to adaptive data analysis. In Silvia Chiappa and Roberto Calandra, editors, *Proceedings of the Twenty Third International Conference on Artificial Intelligence and Statistics*, volume 108 of *Proceedings of Machine Learning Research*, pages 2830–2840, Online, Aug 26–28 2020. PMLR.
- Daniel Russo and James Zou. Controlling bias in adaptive data analysis using information theory. In Arthur Gretton and Christian C. Robert, editors, *Proceedings of the 19th International Conference on Artificial Intelligence and Statistics*, volume 51 of *Proceedings of Machine Learning Research*, pages 1232–1240, Cadiz, Spain, 09–11 May 2016. PMLR.
- Shai Shalev-Shwartz and Shai Ben-David. *Understanding Machine Learning: From Theory to Algorithms*. Cambridge University Press, USA, 2014. ISBN 1107057132.
- Susanne Still, David A Sivak, Gavin Bell, and Gavin E Crooks. Thermodynamics of prediction. *Physical Review Letters*, 109(12):120604, 2012. doi: 10.1103/PhysRevLett.109.120604.
- Richard S. Sutton and Andrew G. Barto. *Reinforcement Learning: An Introduction*. The MIT Press, Cambridge, MA, second edition, 2018.
- A B Tsybakov and Vladimir Zaiats. *Introduction to Nonparametric Estimation*. Springer Series in Statistics. Springer, New York, New York, Dec 2009.
- Vladimir N. Vapnik. *Statistical Learning Theory*. Wiley, New York, 1998. ISBN 978-0-471-03003-4.
- Martin J. Wainwright. *High-Dimensional Statistics: A Non-Asymptotic Viewpoint*. Cambridge Series in Statistical and Probabilistic Mathematics. Cambridge University Press, Cambridge, UK, 2019.
- Aolin Xu and Maxim Raginsky. Information-theoretic analysis of generalization capability of learning algorithms. NIPS’17, page 2521–2530, Red Hook, NY, USA, 2017. Curran Associates Inc. ISBN 9781510860964.
- Bin Yu. *Assouad, Fano, and Le Cam*, pages 423–435. Springer, New York, New York, 1997. doi: 10.1007/978-1-4612-1880-7_29.
- Peng Zhao, Yu-Jie Zhang, Lijun Zhang, and Zhi-Hua Zhou. Adaptivity and non-stationarity: Problem-dependent dynamic regret for online convex optimization. *Journal of Machine Learning Research*, 25(98):1–52, 2024.
- N. N. Čencov. *Statistical Decision Rules and Optimal Inference*, volume 53 of *Translations of Mathematical Monographs*. American Mathematical Society, Providence, RI, 1982. ISBN 978-0-8218-4502-8.